U.PORTO
FEUP FACULDADE DE ENGENHARIA
UNIVERSIDADE DO PORTO

# Ply thickness effects on onset and propagation of transverse cracking: thermoplastic and thermoset-based composites

Ana Rita Moreira Ribeiro

Thesis submitted to Universidade do Porto – Faculdade de Engenharia
in partial fulfilment of the requirements for the degree of
Master in Mechanical Engineering

Supervisor
Professor Carolina Furtado Pereira da Silva
Professor Federico Danzi

Mestrado Integrado em Engenharia Mecânica (MIEM)
Departamento de Engenharia Mecânica (DEMec)
Faculdade de Engenharia (FEUP)
Universidade do Porto (UP)

# Acknowledgements

Firstly, I want to express my gratitude to my mentor and supervisor, Professor Carolina Furtado, whose knowledge, availability, patience, and support were essential to the development and to elevate the quality of my work.

To Professor Federico Danzi, I am grateful for all the valuable suggestions that were crucial for my work. I appreciate the guidance, experience, and encouragement provided throughout the last months. To Eng. Pedro Campos who helped me throughout the semester was always available to help with the experimental tests program and to provide advice that contributed to the outcome of this work.

To all my closest friends and course mates, I am grateful for the countless afternoons spent studying; for the conversations about our separate dissertation topics that still managed to enhance our work; for the encouragement provided when I doubted myself the most; and above all, for your friendship and companionship through the last five years.

I cannot forget to thank the whole FEUP Formula Student Team, for making the last three years particularly special. Thank you for the companionship, for pushing me to the maximum and above all for the friendships made.

Finally, I would like to thank my family who always supports me, my parents, for the affection and wise words at the right moments, and for encouraging me to commit myself to everything I do. To my brother for always having been by my side, for having helped me in the moments when I most doubted if I would be able to finish this journey.

Thank you very much, to all of you!

# Abstract

The move from thermoset-based materials to thermoplastic-based materials represents a significant change in the development of composite materials in the aerospace industry. Therefore, understanding the damage behaviour of these materials is essential to ensure their reliable performance and durability. Transverse cracking in multidirectional composite laminates under tensile loading is typically the first failure mechanism observed and its study has great importance for predicting laminate failure. Thus, the study of the onset and propagation of transverse cracking para thermoplastic and thermoset-based composites is presented in this work, with emphasis on the effect of the transverse ply thickness.

To achieve this goal, experimental analysis of two thermoplastic and two thermosets under tensile loading was carried out to capture the evolution of crack propagation through in-situ imaging. Additionally, analysis of the images obtained through *in-situ* synchrotron radiation computer tomography testing was performed for one of the thermoplastic materials, enabling more detailed information on internal damage through volumetric analysis. Regarding the difference between the two types of materials, the higher toughness of the thermoplastic matrix resulted in a less pronounced influence of the transverse ply thickness effect on the obtained results. Additionally, it led to a slower formation of cracks.

Through the analysis of *in-situ* synchrotron radiation computer tomography images, the determination of volumetric damage percentage was obtained, revealing an increase in damage with increasing transverse ply thickness. The propagation of transverse cracks within the material is not uniform, and therefore, the analysis of transverse damage at the material's edge may not fully correspond to what is observed internally, leading to potential overestimation. With the increase in ply thickness, a more uniform distribution of cracks in the thickness direction and within the material's interior is observed.

**Keywords:** Composite materials, Transverse Matrix Cracking, Ply Thickness, Thermoplastic Composites, Thermoset Composites, Mechanical Testing, Synchrotron Radiation Computed Tomography Analysis.

# Contents

# List of Figures

# List of Tables

# Chapter 1

# Introduction

The aeronautical industry, driven by the pursuit of competitive solutions to thrive in such an ever-evolving field, constantly searches for greater efficiency and innovative solutions for their products. In this context, process optimization, cost and weight reduction, e.g. through the development of advanced materials, are critical factors for the success of the industry. Composite materials have been studied over the last few years for this purpose due to their high specific strength, excellent mechanical properties, and tailorability [1].

Composite materials were first used in some elements of military aircraft in the 1960s and in commercial aircraft in the 1970s. Over the years and development of these materials grew and they are now used in both secondary and primary aircraft structures. Most recent aircraft designs already feature a large number of composite material structures, including wing panels and fuselage, which represent approximately 50 % of the overall structural weight.

Thermoset composites have been the primary choice for the early development of composite structures. However, parallel to improve efficiency through the use and development of improved manufacturing processes and design techniques, sustainability has become a major priority of the transportation industries. For this reason, during the 2010s, one of the most significant developments has been the development of thermoplastic-based composites and the development of manufacturing processes compatible with these materials. These materials have emerged as a more compelling alternative to traditional thermoset polymers, as high-performance thermoplastic resins, besides comparable performance to the thermoset resins, offer higher toughness, near-infinite shelf life (leading to significant reductions in manufacturing costs when compared to thermoset composites which have to be stored at very low temperatures [2, 3]), recyclability opportunities, and the possibility of using joining and manufacturing techniques more compatible with large production rates as thermoforming and welding (as thermoplastic polymers can be softened by heat, melted, and reshaped repeatedly as desired).

Composites are heterogeneous and non-isotropic materials with complex failure mech-

anisms due to the different properties of the constituents, the different fibre orientations and stacking sequences and the specific response to different types of loading. The most common damage mechanisms in composites are matrix cracking, fibre fracture and delamination. Due to the complexity of the composite structure, damage initiation is often not detectable at the visible surface of the structure, making it critical to understand the influence of each of the different mechanisms on the ultimate failure of the material. The first failure mode is usually the initiation of micro-cracks in the matrix through the thickness of the laminate, resulting in a decrease in the material's toughness and consequently leading to the loss of its structural integrity even before the onset of fibre breakage.

Understanding the failure mechanisms and damage behaviour of composite materials is fundamental to ensure their reliable functionality and durability in various applications, such as aeronautics, where composite materials are currently widely used and the repercussions of structural failure can be catastrophic. The initiation and propagation of transverse cracking, which can occur due to various loading scenarios, is one of the most prevalent failure mechanisms in composite materials and has been thoroughly analysed in the context of thermosetting composites. However, due to the increasing use of thermoplastic-based composites in aeronautic applications, it has become increasingly imperative to examine the initiation and propagation of transverse cracking in these materials as well. A proper understanding of the failure mechanisms of thermoplastic-based composites is critical for their efficient and safe use. In this study, the author aims to contribute to the understanding of the failure mechanisms of thermoplastic composites, focusing on matrix cracking under tensile loads.

## 1.1 Objectives

The main aim of this dissertation is to study the effect of ply thickness on the initiation and propagation of transverse cracking in thermoplastic and thermosetting polymer matrix composite materials. In this way, the analysis of the behaviour of cross-ply laminates under tension is done allowing the study and comparison of the behaviour of both materials, in order to understand the behaviour of thermoplastic materials given the great demand for a transition to recyclable materials.

## 1.2 Thesis layout

This dissertation has been organised in such a way that a perceptible reading bearing in mind the described objectives:

In Chapter 1 a brief introduction to the proposed theme is presented along with the goals defined for this project.

In Chapter 2, the state of the art regarding the study of transverse matrix cracking is presented. An introduction is made concerning the basic notions of composite materials, focusing on thermoplastic and thermosetting polymer matrix composite materials.

Subsequently, the main failure mechanisms are presented and, finally, the state of the art concerning the effect of layer thickness on the behaviour of fibre-reinforced composite laminates, focusing on the experimental analysis performed so far based on the available literature.

In Chapter 3 the procedures relating to the experimental program carried out are described. Two thermoplastic and two thermoset materials were used in the analysis, for which the properties are presented. The preparation of the specimens and the tensile test performed are also described in this chapter.

The results obtained from the tests described in the previous chapter and their corresponding analysis are presented in Chapter 4 of this report. The analysis has as its main focus the analysis of the stress curves obtained and the images captured during the various tests. The study of crack density and crack spacing evolution are presented in detail focusing on the effect of transverse ply thicknesses.

In Chapter 5, in complement to the analysis performed considering the experimental tests, the analysis of the results obtained after in situ DENT test using Synchrotron Radiation Computed Tomography was performed for one of the thermoplastic materials studied in Chapter 4. The analysis of the influence of transverse ply thickness is defined by studying the evolution of the damage volume.

To finalize, in Chapter 6, the conclusions obtained from the analysis are exposed together with proposed future work that will enrich the presented work.

# Chapter 2

# State-of-art and Literature Review

An introduction to composite materials, with particular emphasis on thermoset and thermoplastic-based composites, is presented in this chapter. Then, the various failure mechanisms inherent to laminated composites are presented. Finally, the effect of ply thickness on the mechanical behaviour of multidirectional composite laminates, with a focus on matrix cracking and in-situ effect, is analyzed, along with a succinct overview of relevant experimental studies.

## 2.1 Composite Materials

Composite materials are obtained by the combination of two components with different characteristics: the reinforcement, which can be continuous or discontinuous and is responsible for the strength and stiffness of the material, and the matrix, which surrounds the reinforcements, ensures material cohesion. Given the diversity of the constituents, different types of composites can be formed based on the type of reinforcement and the matrix used. The type of reinforcement can be made of continuous or discontinuous fibres or particles, while the matrix can be metal-, ceramic- or polymer-based.

### 2.1.1 Polymer Matrix Composites

The most commonly used composites in the aeronautical industry are continuous carbon fibres with a polymeric matrix. Fibre-reinforced polymer composites are characterized by their excellent mechanical properties, where the polymer resin presents an isotropic behaviour, however, the fibres present a transversal isotropic behaviour with a higher strength in the fibre direction concerning the perpendicular direction [4, 5]. Polymeric Matrix Composites (PMCs) can be classified into two main groups, namely thermoset-based composites and thermoplastics-based composites (Figure 2.1).

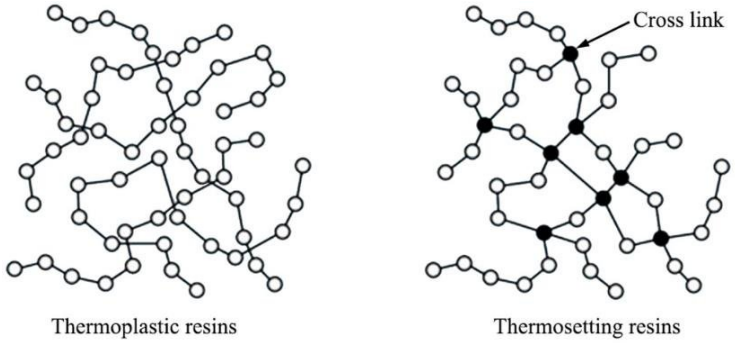


**Figure 2.1:** Molecular structure of thermoset and thermoplastic polymers [6].

Thermoset-based composites are characterized by the formation of an irreversible cross-linked three-dimensional network during the resin cure process through heat and chemical reactions involving the exchange of electrons. These covalent bonds formed after the polymerization process result in a permanent network that cannot be reformed, making the reprocessing of thermoset resins or their recycling extremely complicated. However, due to their high temperature and chemical resistance, high dimensional stability, and strong and rigid structure, these materials find widespread use in various industries. The high toughness of the thermosets is often accompanied by low transversal fracture toughness, transverse tensile, and low interlaminar tensile and in-plane shear failure strains, making them susceptible to micro-cracking. The various types of thermosetting polymers are classified based on their chemical configuration, such as polyesters, vinylesters, epoxies, phenolics, polyamides, and bismaleimides [7–9].

In contrast to thermoset-based composites, thermoplastics-based composites do not form irreversible cross-linked networks during the manufacturing process. This allows them to be reshaped with the increase in temperature, making their recycling and reprocessing much easier. The manufacturing process of thermoplastics is achieved by melting, consolidation and cooling the resin, which results in high tensile strength, stiffness, and dimensional stability, good compression and fatigue strength, and high durability and damage tolerance. The most commonly used thermoplastic resins include polypropylene (PP), polyvinylidene fluoride (PVDF), polymethyl methacrylate (PMMA), polyphenylene sulfide (PPS), polyetherimide (PEI), and the Poly(aryletherketones) (PAEKs). Resins from the PAEK family, such as polyetheretherketone (PEEK) and polyetherketoneketone (PEKK), have garnered significant interest in the aeronautic industry due to their excellent properties. PEEK is the most commonly used thermoplastic, however, due to its high processing temperature, the need arose to search for a new candidate. PEKK has been studied over the last few years as it has excellent mechanical, thermal, and chemical properties with a lower glass transition temperature and processing temperature than PEEK [2, 3].

### 2.1.2 Manufacturing processes of polymer fibre reinforced composites

The manufacturing process has a significant impact on the properties and performance of composite materials. Deviations, incomplete curing or improper processing can lead to defects such as voids, resin-rich areas, and poor interfacial bonding between matrix and fibres, resulting in inferior properties, and reduced durability, affecting the overall quality and reliability of the composite structure.

The most common manufacturing process for thermoset composites is the autoclave process which consists of a high-temperature and pressure process, enabling a chemical curing reaction for geometry stabilisation during forming. This process uses lay-up prepreg, consisting of fibre plies pre-impregnated with resin, vacuum bag forming and autoclave curing. The resin curing process is initiated and maintained by increasing the temperature. The compaction of the laminate to the desired fibre volume fraction and the voids elimination during curing is achieved by applying pressure [10–12].

For thermoplastic-based composites, the most commonly used process is compression moulding, which involves a two-part mould that is heated when closed. The final temperature must be higher than the crystalline melting point, $T_m$, to reach the liquid stage and allow for the reshaping of the component. Once moulded, the mould is cooled and crystallization occurs between the melting temperature, $T_m$, and the glass transition temperature, $T_g$ [9, 13]. The level of crystallinity attained during processing present a crucial role in the mechanical properties of the composite. The polymer matrix in thermoplastic composites can be semi-crystalline or amorphous, and the level of crystallinity can be controlled by processing conditions, such as the cooling rate, processing temperature, and applied pressure. Higher cooling rates lead to higher levels of amorphousness, while lower cooling rates result in higher degrees of crystallinity. Furthermore, higher processing temperatures and pressure can promote crystallization, increasing stiffness and strength.

Regarding PEKK-based composites, the T/I (terephthalic/isophthalic) ratio is also an important parameter that can significantly affect the degree of crystallinity and consequently the properties and processing characteristics of the component. With the presence of terephthalic acid units occurs the formation of a more ordered crystalline structure, resulting in a higher crystallinity in the composite. In contrast, with the presence of isophthalic acid units results in a disruption of crystal formation, leading to a lower crystallinity [2, 14].

## 2.2 Failure Mechanisms

Laminated composite materials are heterogenous and anisotropic in nature and their damage mechanisms depend on the scale under analysis: microscale (where the fibres and matrix elements are considered), mesoscale (ply level), or macroscale (laminate level). At the mesoscale, the ply is considered homogeneous and the ply is considered transversely isotropic [15].

At this level, the damage mechanisms can be defined as intralaminar, which includes matrix cracking, fibre failure (breaking and kinking) or fibre-matrix shear interface, or as interlaminar, delamination (Figure 2.2). Generally, matrix failure occurs first, followed by fibre failure, which controls the final failure of the material [16, 17].

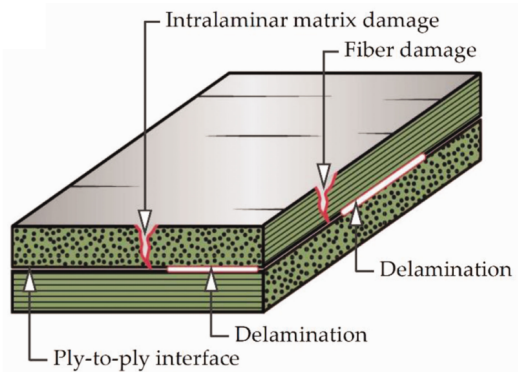


**Figure 2.2:** Failure mechanisms in laminates [18].

### 2.2.1 Fiber Failure

When the material is subjected to tensile loads in the longitudinal direction, the force is distributed between the fibres, until a fibre breaks. Fibre failure is a statistical process, dominated by defects in the fibres. After the first fibre breaks, the stresses are redistributed and the process is repeated. When a sufficiently large cluster of broken fibres occurs, the ply fails, and its load carrying capability is lost [19].

Under a longitudinal compressive load, failure occurs due to local bending of the fibres caused by local fibre misalignment, which may lead to deformation in ductile fibres or fracture in brittle fibres. The presence of shear stresses leads to further misalignment of the fibres and consequently results in the creation of a kink band [19, 20].

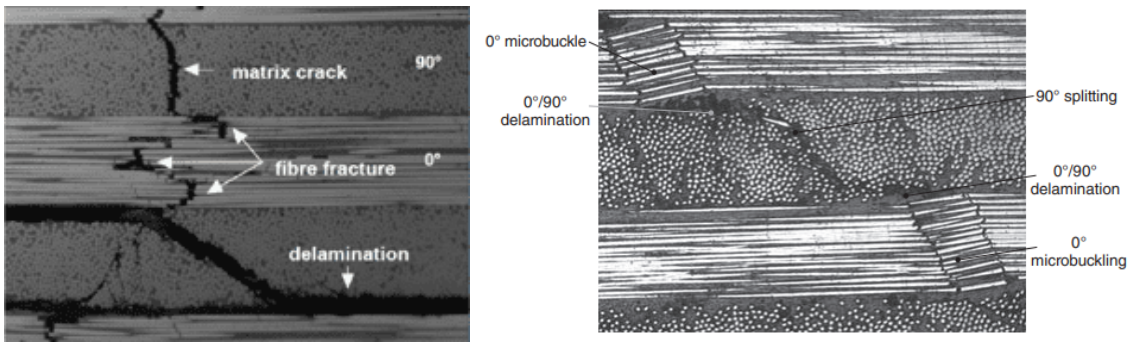


**(a)** **(b)**

**Figure 2.3:** Failure modes under: a) Tension loading [21], b) Compression loading (adapted from [22]).

### 2.2.2 Matrix Failure

Matrix cracking is a type of damage commonly observed in composite laminates, especially in transverse plies under tension, mainly as a result of their tensile strength is lower than that of 0 plies. Matrix cracking in the 90° plies can increase the load carried by the 0 ° plies and introduce stress concentration at the crack tip, eventually leading to fibre failure and laminate failure [19, 23].

Several studies have been carried out on transverse cracking in multidirectional composite laminates focusing on cross-layer laminates with a 0° layer as an outer layer and a 90° layer on the inside. The strength of a 90°lamina depends on the restraining effect of the adjacent plies, and as the load is increased, more cracking and an increase in crack density to saturation occur. The introduction of internal damage and cracks in the matrix can significantly decrease the effective stiffness of the cracked plies, causing a stress redistribution in the structure and a decrease in the modulus of elasticity of the laminate [23–25].

The evolution of transverse cracks can be divided into 3 phases:

- First, crack initiation and propagation across the width occurs. Crack initiation is a statistically-driven phenomena consequence of the inherent variability in the local fracture toughness of the matrix material, which is often attributed to manufacturing defects such as voids, incompletely cured regions, inclusions, and weakly bonded fibre-matrix interfaces. Consequently, the initial cracks that form from these defects may exhibit randomness in their location, size, shape, and growth rate during the early stages of damage development.
- Then, the stress in the ply is redistributed, and other cracks appear in other locations. The crack density increases with the increasing load. The crack appearance rate is rapid in the beginning of the process and slows down as the maximum number of cracks is reached.
- Finally, the evolution of the cracks reaches saturation leading to other types of damage, as delamination and fibre breakage.

The evolution of matrix cracking can be quantified by experimentally measuring the number of cracks per unit length, referred to as crack density. The first cracks created are distributed randomly in the specimen, while with increasing density it is possible to verify a more uniform distribution. The prediction of the new failure position can be performed using probabilistic analytical models, based on the critical energy release, as studied by several authors [26–28].

### 2.2.3 Delamination

When the various failure modes of the lamina are combined at the laminate level, the generation of matrix failure in the different plies will result in increased stresses near the interface between the plies resulting in their separation. This phenomenon is named

delamination[29].

Carraro et al. [29], studied that delamination in composite laminates can occur through different mechanisms. The most common mechanisms of delamination onset related to are through the presence of transverse cracks that reach the interface in the straight or branched configuration as it is possible to observe in figure 2.4. The occurrence of delamination without the presence of transverse cracks was also observed due to irregularities on the edge surfaces. It was concluded that the onset of delamination occurs at a much higher load in laminates with thinner transverse plies.

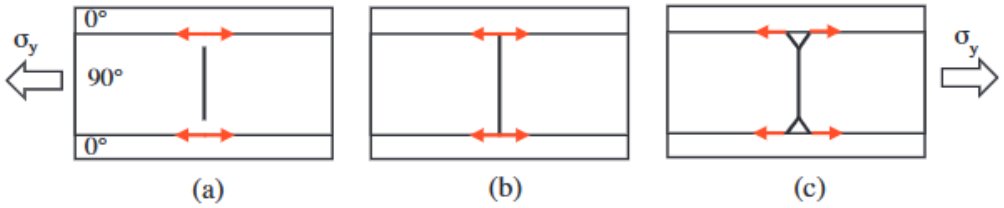


**Figure 2.4:** Delamination initiation mechanisms a) Cook-Gordon mechanism, b) straight, and c) branched [29].

## 2.3 Ply Thickness Effect in Composite Laminates

In multidirectional laminates, the onset and propagation of transverse cracks in lamina with perpendicular orientation to the load occur at strain levels lower than the failure strain of the laminate. These mechanisms are the most recurrent ones and cause material degradation at the ply, which can propagate to the interlaminar region (delamination), accelerating the final failure of the laminate.

It has proved that the failure strength of transverse layers embedded in a multidirectional laminate is higher than that of unidirectional laminate, due to the constraints imposed by the adjacent layers that result in a delay in the crack initiation. The ply thickness also influences the matrix-dominated ply strengths and the crack density: the thinner the ply, the higher the strength and crack density in the ply [30–32]. This ply thickness effect is known as the *in-situ* effect [17, 33–35].

In order to evaluate the effect of ply thickness on the determination of the onset and propagation of transverse cracking it is possible to consider the *in-situ* effect using fracture mechanics models. As important properties to consider for this study are the fracture resistance and *in-situ* strengths in order to define failure criteria for the prediction of transverse damage mechanisms in multidirectional laminates [24, 25, 36].

### 2.3.1 Effect of ply thickness on the crack density evolution and ply strength

Garrett and Bailey [37], Bailey and Parvizi [30], Parvizi et al. [38] carried out the first experimental studies on the effect of ply thickness of 90° layers. They studied cracking on-

set and propagation on 90° layers with different thicknesses (0.1 to 4 mm) when embedded between $0^{o}$ plies with a fixed thickness under tensile loads. In these studies, the relationship between the transverse crack spacing, the 90° ply thickness and the applied stress were analysed: with the decrease of the thickness of the 90° ply, a decrease of the crack spacing was observed (Figure 2.5a). Additionally, the relation between the ply thickness and the onset transverse crack strain was studied: for thinner ply thicknesses, the cracks are not visible prior to failure, for intermediate thicknesses small edges cracks appear at a higher strain and grow slowly, and for thick ply, with a thickness superior to 0.4 mm, the growth occurs instantaneously ( Figure 2.5b).

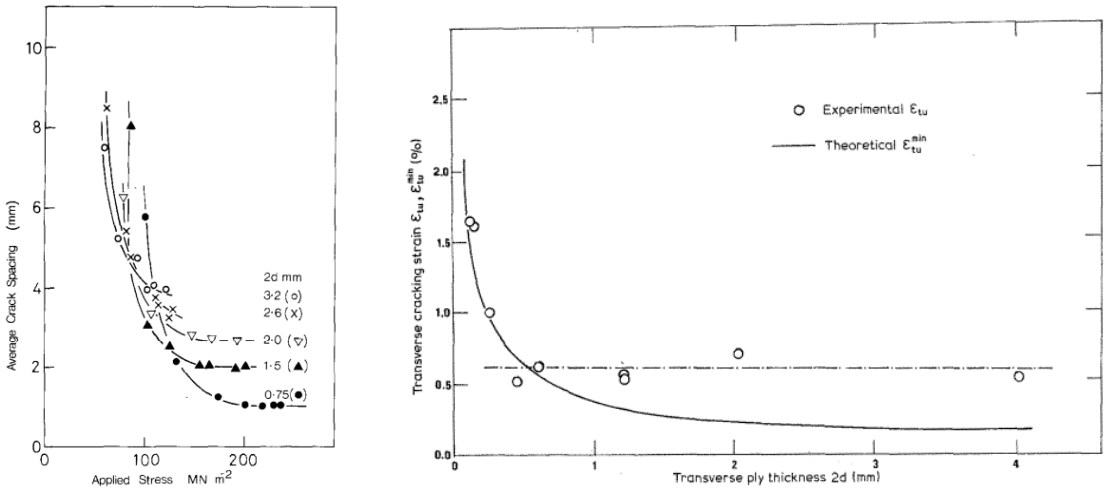


**(a)** **(b)**

**Figure 2.5:** a) Relation of crack spacing with the transverse ply thickness and the applied stress [37], b) Relation of the onset transverse cracking strain with the transverse ply thickness [38].

Following the study carried out by the previous authors, Flaggs and Kural [31] concluded that, in addition to the effect of transverse ply thickness, the orientation of the outer layers has an influence on the strain and stress value of the onset transverse crack. Tensile tests were performed considering Graphite/Epoxy $[\pm\theta/90]_s$ laminates, with $\theta$ equal to 0°, 30° and 60°. In this research, it was referred for the first time to the existence of the *in-situ* effect on the transverse tensile strength (Figure 2.6).

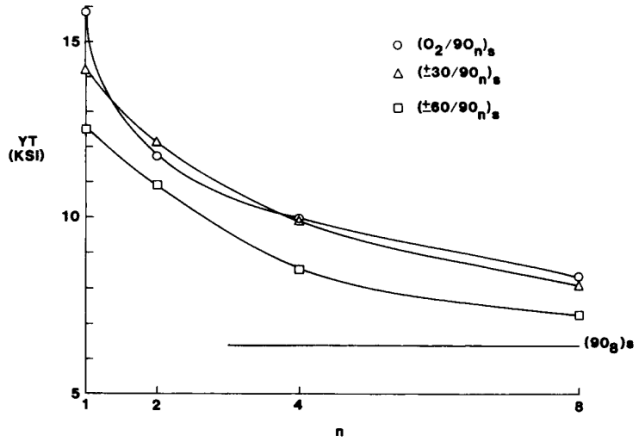


**Figure 2.6:** Relation between the thickness of the transverse ply, the orientation of the constraints plies and the *in-situ* transverse strengths [31].

The evolution of the crack density due to applied stress during a static tension loading was studied by Liu and Nairn [39] for a Graphite/Epoxy laminate and a Carbon/PEEK laminate of configuration $[0_m/90_n]_s$ varying the number of layers of 90∘ and 0∘. For low applied loads, a slow increase of the crack density with the increase of the applied load was observed. After the appearance of the first cracks, an exponential increase of the crack density until saturation is reached and delamination initiates were observed. At this point, the crack density versus applied stress becomes constant (Figure 2.7).

Boniface et al. [40] carried out an analysis on notched and unnotched specimens varying the number of the 90° layers in the laminates. The author observed that the transverse cracking failure process can be divided into two distinct stages: initiation and propagation. For the specimens with a thicker transverse ply, the crack propagation through the thickness and width occurs instantaneously after initiation. The same is not observed for the thinner plies, where there is higher resistance in both stages of crack evolution.

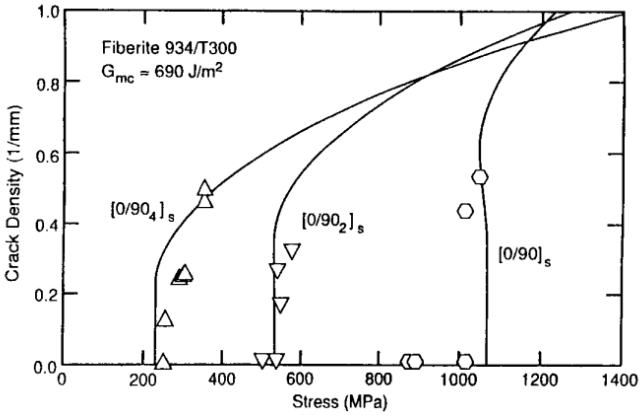


**Figure 2.7:** Crack density vs applied load in Graphite/Epoxy cross-ply laminates [39].

### Crack Spacing Analysis

The previously mentioned studies [26–28] focused on the formation of transverse matrix cracks in cross-laminated laminate and on increasing the understanding of crack density evolution. This was considered assuming a uniform spacing between cracks. However, the crack distribution might not always be uniform, particularly in the presence of material defects, such as micro-crack, voids or weak interface zones between the fibres and the matrix. Therefore, to enrich the analyses, not only crack density but also crack spacing was studied by several authors [25–28, 41] with the purpose of developing models that represent crack density more accurately.

Laws and Dvorak [25] proposed a progressive damage model for transverse cracking in cross-ply composites, utilizing the shear lag model. The model defined yielded good predictions for stiffness reduction in the laminates and allow an analysis of progressive matrix cracking. For this study, three cases were considered for the creation of new transverse cracks between consecutive cracks, incorporating different failure probability functions. In the first case, it was assumed that the next crack was guaranteed to occur at the midpoint. The second implied that all locations between the two previous cracks were equally probable. The third, based on simple fracture mechanics, considered the position of the next crack to be proportional to the stress in the transverse ply. Despite the similarity to the experimental results, the appearance of random cracks outside the region considered led to the need to develop different methods. With the intention of accounting for material flaws, some non-deterministic models have been studied.

Aiming to consider the random patterns of crack distribution, Silberschmidt [41] defined four spacing models, three considering a uniform distribution with a maximum, minimum and average spacing and one considering a random distribution based on the Weibull distribution (Figure 2.8). The analysis was performed on carbon-fibre epoxy resin cross-ply laminates $[0_m/90_n/0_m]$ to determine an approximate function for the crack spacing. Using X-ray analysis it was possible to define a Weibull distribution function with three parameters. Based on these results, it could be concluded the influence of crack spacing on the stress distribution, noting the importance of performing studies considering uniform and non-uniform spacings, allowing the obtaining of a more consistent analysis in laminates with different orientations.

These models allow a probabilistic analysis of the new crack initiation location. The above methods will not be used in the present study, nevertheless, they are included as an introduction to the study of average crack spacing.

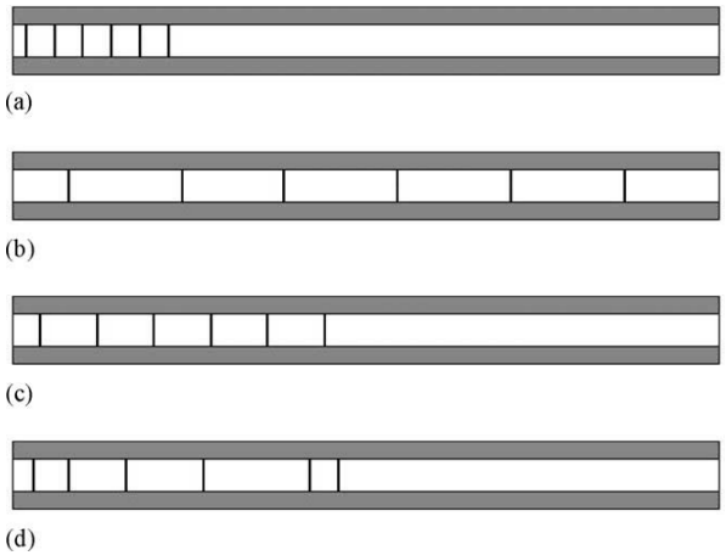


**Figure 2.8:** "Four cases of modelled crack spacings: minimum (a), maximum (b), mean (c), and random (d)." Figure and description from [41].

**Analytical prediction of the ply strength as a function of the ply thickness**

To analytically predict the transverse and in-plane shear ply strengths (defined as the stress at which the first matrix crack is formed) as a function of the ply thickness, analytical models based on Fracture Mechanics were developed over the.

Based on the theory of Aveston and Kelly [42] to analyse the formation of multiple cracking in unidirectional fibre-reinforced composites, Parvizi et al. [38] developed a modified shear lag model to analyze the onset and propagation of transverse cracking in cross-ply laminates. Through the combination of the one-dimensional shear-lag analysis and the Griffith energy concept, the authors determined the value of the minimum transverse failure strain, known as in-situ transverse failure strain, which can be described by:

$$\epsilon_{\mathrm{tu}}^{\mathrm{min}} = \sqrt{\frac{2bE_1\gamma_{\mathrm{t}}\phi^{1/2}}{(b+d)E_{\mathrm{t}}E_{\mathrm{c}}}}, \tag{2.1}$$

with

$$\phi = \frac{E_{\mathrm{c}}G_{\mathrm{t}}}{E_{\mathbf{1}}E_{\mathrm{t}}}\frac{b+d}{bd^2}. \tag{2.2}$$

This method presented limitations due to the consideration only in mode 1 of failure, discarding the effects of in-plane shear stresses in the formation of the cracks [31]. To address this limitation, Flaggs [43] proposed a new approach for the prediction of tensile matrix failure by combining the two-dimensional shear-lag analysis with the mixed mode strain energy release rate fracture.

Dvorak and Laws [25, 26] defined the first ply failure based on the propagation of the crack in the fibre axial and perpendicular directions by appealing to a slit crack occurrence. Thus, it was suggested a criterion for cracking prediction of a matrix based on fracture mechanics, considering the effect of blade thickness under in-plane shear stresses and transverse tensile stresses. In this paper, was shown that for thicker plies the initial cracks will not lead to an instantaneous effect on the adjacent plies, since the flaw is formed in the ply centre. On the other hand, the formation of cracks on thinner plies will lead to an instantaneous effect, due to the fact that their length will more limited by the adjacent plies.

Camanho et al. [24] proposed an analytical model to predict *in-situ* under transverse tension and in-plane shear that accounts for ply position (embedded within a laminate, or surface ply) and ply thickness. This approach relies on the energy exchange between a layer and an elliptical fracture, considering the crack growth in the perpendicular and parallel directions developed by Dvorak and Laws [25]. For this analysis, three possible configurations were considered to determine the *in-situ* strengths, represented in figure 2.9.

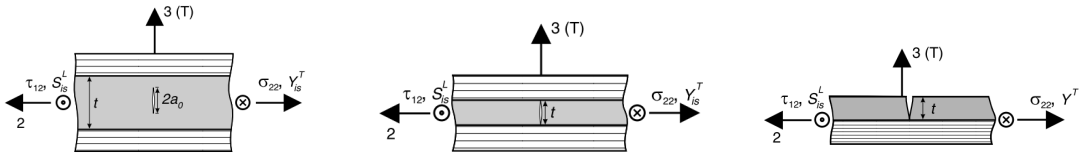


**(a)** **(b)** **(c)**

**Figure 2.9:** a) Thick transverse ply thickness, b) Thin transverse ply thickness, c) Thin outer ply thickness [24].

# Chapter 3

# Experimental Part

The aim of this work is to analyse the effect of ply thickness on the initiation and propagation of transverse cracks in composite materials of different polymeric matrix types and grade. For this purpose, four material systems were experimentally tested: two thermoplastic-based and two thermoset-based composites. Each material was analysed considering a cross-ply laminate varying the number of layers of the cross laminae. In this chapter, the aspects related to the materials used, the specimen preparation and the tests performed will be presented.

## 3.1 Material

The four materials analysed consist of carbon fibre and polymeric matrix, namely two thermoset-based composites consisting of Epoxy resin matrix and two thermoplastic-based composites consisting of PEEK resin matrix.

- The Thermoset A is a T800/736LT, a thin-ply carbon/epoxy prepreg with a fibre areal weight of 50 g/m$^2$ supplied by North thin-ply Technology (NTPT). Its nominal cured ply thickness is 0.052 mm [44]. The curing cycle consisted of heating the plates to the dwell plateau at 70°C for one hour and full cure for 45 minutes at 120°C.
- The Thermoset B is a T700/FRVC411, a flame retardant carbon/epoxy prepreg with a fibre areal weight of 140 g/m$^2$. Its nominal cured ply thickness is 0.153 mm [45]. The curing cycle consisted of heating the plates to the dwell plateau at 70°C for one hour and full cure for 45 minutes at 120°C.
- The Thermoplastic A is composed of unidirectional APC-2 AS4/PEEK thermoplastic tapes. The consolidation process was performed by hot pressing using a Wickert hydraulic press with conditions to ensure a high crystallinity level in the composite (30%).

Regarding thermoplastic material B, its composition and consolidation process cannot be presented in this work for confidentiality reasons. The elastic properties of the

materials used in this project are summarized in tables 3.1, 3.2 and 3.3, for Thermoset A, B and Thermoplastic A, respectively, where $E_1$ is the longitudinal elastic modulus, $E_2$ the transversal elastic modulus, $G_{12}$ the shear modulus and $\upsilon_{12}$ the in-plane Poisson ratio.

**Table 3.1:** Elastic Properties of Thermoset A

| $E_1$ (GPa) | $E_2$ (GPa) | $G_{12}$ (GPa) | $\upsilon_{12}$ |
|---|---|---|---|
| 143.83 | 7.853 | 3.803 | 0.378 |

**Table 3.2:** Elastic Properties of Thermoset B

| $E_1$ (GPa) | $E_2$ (GPa) | $G_{12}$ (GPa) | $\upsilon_{12}$ |
|---|---|---|---|
| 102 | 6.38 | 3.38 | 0.29 |

**Table 3.3:** Elastic Properties of Thermoplastic A

| $E_1$ (GPa) | $E_2$ (GPa) | $G_{12}$ (GPa) | $\upsilon_{12}$ |
|---|---|---|---|
| 147.37 | 10.28 | 5.34 | 0.3 |

The specimens used for the analysis were made of cross-ply laminates, composed by unidirectional ply orientated with configuration $[0_m/90_n/0_m]$. For each material, the number of layers at zero is maintained constant by varying the number of layers at 90°. Four configurations were considered for the thermoset-based composites and three configurations for the thermoplastic-based composites. The configurations analysed are presented in the following tables, as with the nomenclatures used for the identification of the different specimens tested (Table 3.4).

**Table 3.4:** Laminate stacking sequence analysed

| Laminate | Designation | Lay-up | Thickness (mm) | 90° Thickness (mm) |
|---|---|---|---|---|
| Thermoset A | T01 | $[0_6/90/0_6]$ | 0.67 | 0.052 |
| | T03 | $[0_6/90_3/0_6]$ | 0.78 | 0.156 |
| | T06 | $[0_6/90_6/0_6]$ | 0.93 | 0.312 |
| | T12 | $[0_6/90_{12}/0_6]$ | 1.25 | 0.624 |
| Thermoset B | P1 | $[0_2/90/0_2]$ | 0.77 | 0.153 |
| | P2 | $[0_2/90_2/0_2]$ | 0.92 | 0.307 |
| | P3 | $[0_2/90_3/0_2]$ | 1.07 | 0.460 |
| | P4 | $[0_2/90_4/0_2]$ | 1.23 | 0.613 |
| Thermoplastic A | Q3 | $[0_2/90/0_2]$ | 0.66 | 0.132 |
| | Q4 | $[0_2/90_2/0_2]$ | 0.79 | 0.264 |
| | Q5 | $[0_2/90_4/0_2]$ | 1.05 | 0.528 |
| Thermoplastic B | M1 | $[0_3/90/0_3]$ | 1.33 | 0.190 |
| | M2 | $[0_3/90_2/0_3]$ | 1.52 | 0.380 |
| | M4 | $[0_3/90_4/0_3]$ | 1.71 | 0.760 |

## 3.2 Samples Preparation

The materials to be studied were cut with a diamond saw to obtain rectangular specimens with a width of 10 mm, and a height between 130 and 150 mm. After cutting, the central section of the samples was polished through the thickness with Silicon Carbide (SIC) sandpapers with 320-800-1200-4000 mesh to obtain a surface with the necessary finish to visualise the formation of cracks during the subsequent tensile tests.

To provide a better fixation of the samples and to prevent any significant stress concentrations in the section attached to the grips of the test machine, tabs were glued to each sample tested. The tabs used are made of glass fibre with a height of 56 mm and a width of 10 mm. The surface was prepared with fine-grain sandpaper to improve the adhesion of the fibreglass tabs to the samples. Epoxy adhesive HB AS 89/AW 89 was used for attachment.

## 3.3 Tensile Test

All the tests were performed on an Instron 5900R 4208 H 0138-3 electro-mechanical universal testing machine equipped with a 200 kN load cell. The testing machine was equipped with hydraulic grips and the specimens were monotonically loaded in tension at a cross-head speed of 0.25 mm/min while recording force and cross-head displacement. In order to record the failure evolution along the specimen thickness an 18 Megapixel Canon digital camera EOS 80D with macro-lenses was used to monitor a portion of the specimen's thickness.

The images were taken with a time-lapse of 4 seconds, focusing within approximately 20 mm of the edge of the specimen between the grips. For the analysis of the results, the force and displacement readings of the machine were synchronized with the acquisition of the images in order to estimate the value of the applied force in each image.

The tests were carried out in accordance with two different procedures. In the first method, tensile tests were carried out with a continuous increase in load without interruptions until the specimen failed. This method allowed the tensile strength of the laminate to be determined from the relationship between the maximum load before failure and the cross-sectional area of the specimen.

$$X_T^L = \frac{P_{\max}}{A} \tag{3.1}$$

The second method used in the tensile tests consisted of an incremental loading-based analysis. The tests were carried out with stops at pre-stabilised load levels in order to identify the evolution of the transverse cracks and to define the evolution of crack density as a function of the number of plies at 90° and of the material under study. The stop levels were chosen to take into account the strain values of the longitudinal plies since the number of 0° plies is the same for the different configurations of the same material. The

### 3.3. Tensile Test


**Figure 3.1:** Experimental Test Setup used.

strain values can be determined by the equation 3.2, where $A_{0^\circ}$ is the cross-sectional area taking into account the thickness of the longitudinal plies only.

$$\epsilon_{0^\circ} = \frac{P_{\max}}{A_{0^\circ} \times E_1} \tag{3.2}$$

After obtaining the maximum value of stress in the continuous tests, the maximum values of deformation were determined for each laminate analysed. In order to facilitate the comparison of the results, stops were defined taking into account the maximum absolute value of deformation among the different laminates. For this strain value, ten increments were defined, corresponding to the stop points. From the strain values defined for all the laminates, the strength values for each material were defined. As the calculated strain value only takes into account the plies at 0°, this is equivalent for all configurations of each material and the steps are the same for all laminates of each material.

# Chapter 4

# Experimental Results

In this chapter, the experimental results obtained during longitudinal tensile tests of cross-ply laminates for the four materials studied are presented. To study the constraining effect on the influence of the transverse ply thickness for the different laminates, the results are compared between configurations of the same material.

For the analysis of the initiation and propagation of matrix cracks during the tests, the evolution of the damage level in the form of transverse crack density as a function of the applied load was considered. The influence of ply thickness and material type on the initiation and propagation of transverse cracks in the inner 90° layer of cross-ply laminates is also discussed.

## 4.1 Tensile Test

Through the tensile tests, it was possible to obtain the force-displacement curves for each of the laminates investigated, defining the maximum value of the tensile strength and the ratio between the thickness of the 90° layer of the laminate for each material. It is worth mentioning that the preliminary tests were carried out using manual wedge-action grips, which were later replaced by hydraulic grips to ensure a higher clamping force, once slipping was observed.

### 4.1.1 Thermoset A

The results obtained from the experimental tests performed for thermoset A are shown in figures 4.1 to 4.4. From the obtained results, it is possible to observe a reduction in the stiffness of the laminates due to the formation of micro-cracks in the internal layer of the specimens. A variation in the maximum displacement of results in configuration T06 was observed, which can be explained by using different types of grips in the tests, sample 8 was the only one tested with the hydraulic grip. In contrast, the remaining tests were performed with manual grips. Samples 1 and 2 of laminate T03 and 1 to 4 of laminate T12 were tested without tabs although they are shown due to similar behaviour and achieved

the same maximum strength. The specimens with the thinner configuration T01 were all tested considering the procedures mentioned in chapter 2, where the first 3 specimens were tested using continuous loading until failure while and the last 2 specimens were tested in incremental steps.

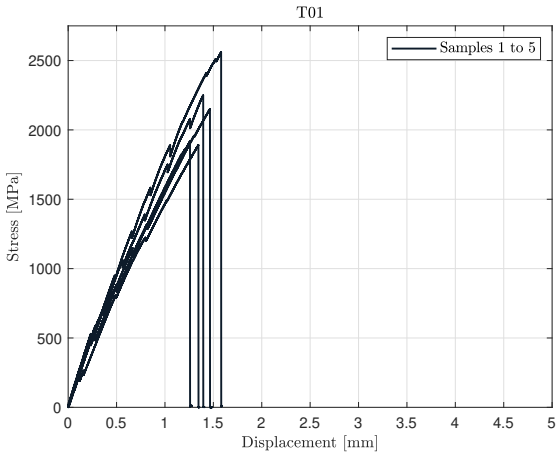


**Figure 4.1:** Stress-displacement tensile test results for configuration with 1 90° ply.

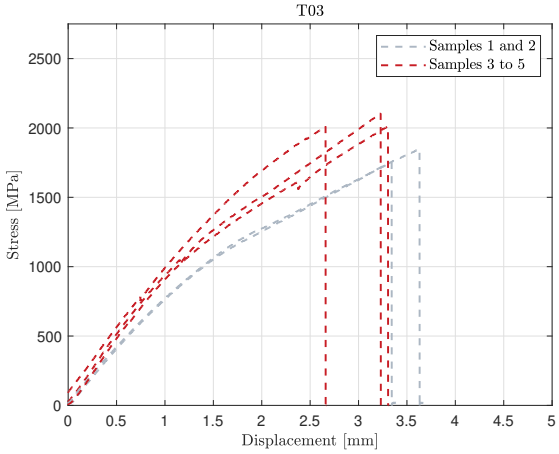


**Figure 4.2:** Stress-displacement tensile test results for configuration with 3 90° plies.

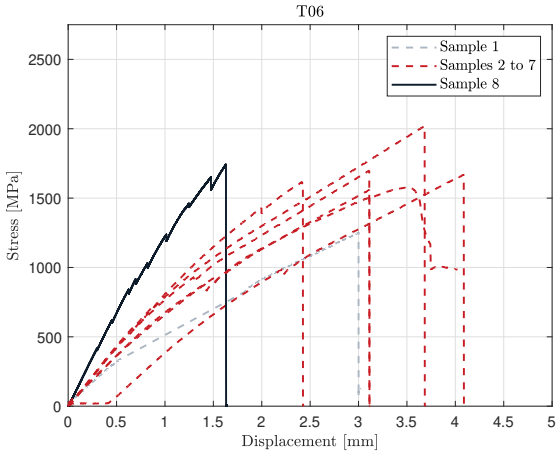


**Figure 4.3:** Stress-displacement tensile test results for configuration with 6 90° plies.

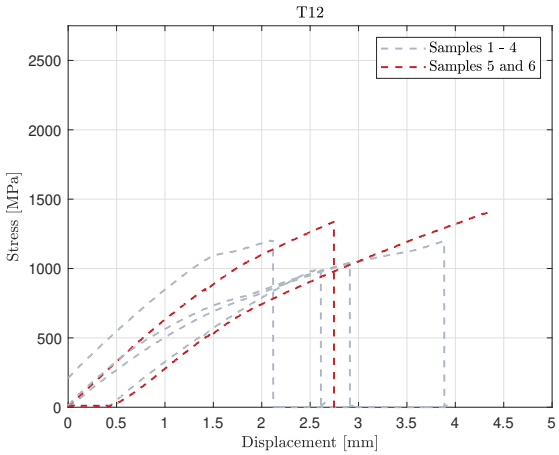


**Figure 4.4:** Stress-displacement tensile test results for configuration with 12 90° plie.

The average tensile strength, $X_T^L$, obtained for the laminate T01, T03, T06 and T012 specimens are shown in table 4.1, along with their coefficient of variation. It should be noted that only the stress values of the specimens in which the test was carried out with tabs and without incremental stops were taken into consideration. While the ultimate tensile strength for the T01 and the T03 results are constant, a remarkable reduction of these properties with the 90° layer thickness can be observed for the T06 and T12 configurations.

**Table 4.1:** Tensile Strength results for the four configuration $[0_6/90_m/0_6]$ of Thermoset A.

| Laminate | Nº of Samples Tested | Tensile Strength $X_T^L$ [MPa] | Coefficient of Variation [%] |
|---|---|---|---|
| T01 | 3 | 1986.32 | 7.14 |
| T03 | 3 | 2041.92 | 2.68 |
| T06 | 5 | 1623.62 | 10.08 |
| T12 | 2 | 1369.78 | 3.39 |

### 4.1.2 Thermoset B

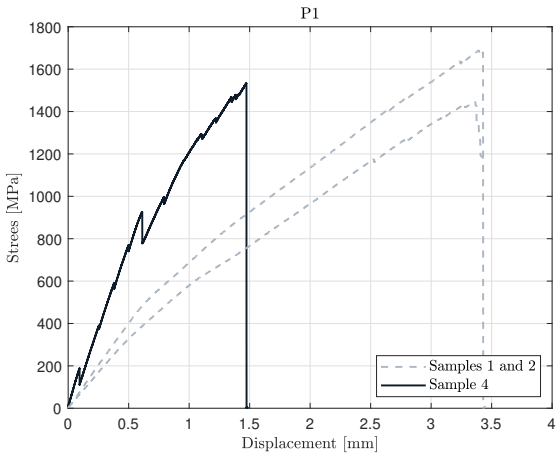


**Figure 4.5:** Stress-displacement tensile test results for configuration with 1 90° ply.

The tensile test results for the thermoset B composite are shown in the stress displacement curves of figures 4.5 to 4.8. Analogously to what was observed in thermoset A, a decrease in stiffness was noticed with increasing load due to the appearance of damage mechanisms, notably matrix cracking and delamination. The first three specimens of the thinner configuration, P1, were tested with the manual grips as well as the five specimens of the P2 configuration and the first two of the thicker configurations, P3 and P4. The curve of the third test specimens P1 and P2 are not represented since the test was stopped after delamination at the interface, without reaching failure.

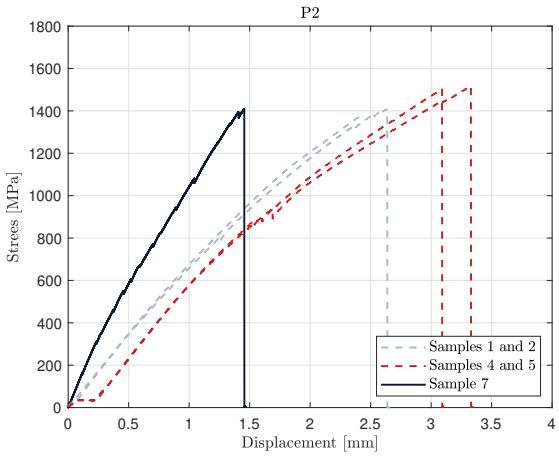


**Figure 4.6:** Stress-displacement tensile test results for configuration with 2 90° ply.

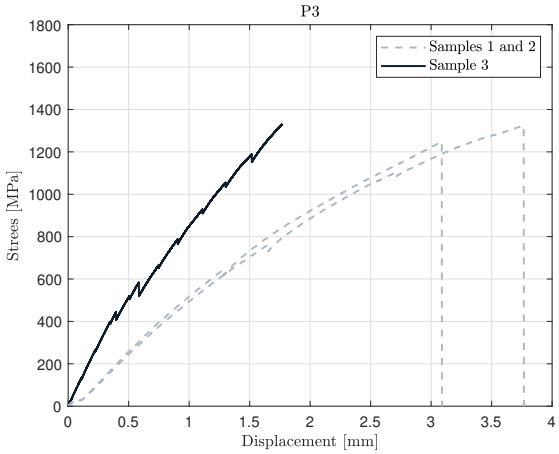


**Figure 4.7:** Stress-displacement tensile test results for configuration with 3 90° ply.

Table 4.2 gives the average values of tensile strength for the different configurations of thermoset B. The highest tensile strength was obtained for the laminate with a lower number of 90° layers. The reduction was 4.58% for the P2 configuration, 16.44% for P3 and 23.47% for the thicker one. The delamination occurred in several tests performed with this material. This effect can be justified by the fact that voids are observed in the samples under optical microscopy during their preparation (Figure 4.9). As studied by several authors [46–50], the presence of voids in the matrix of composite material, when under tension, acts as stress concentrators, leading to pre-cracking function and consequently to premature delamination.

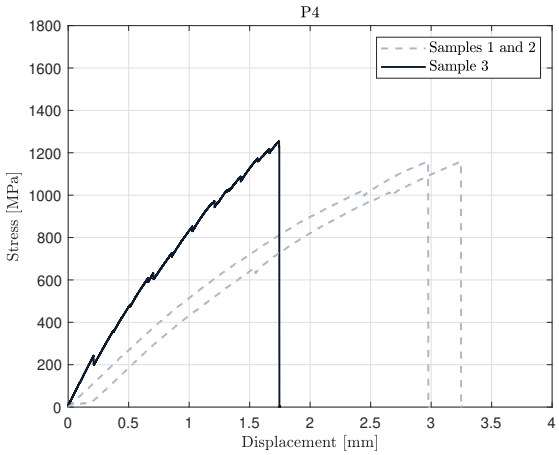


**Figure 4.8:** Stress-displacement tensile test results for configuration with 4 90° ply.

**Table 4.2:** Tensile Strength results for the four configuration $[0_2/90_m/0_2]$ of Thermoset B.

| Laminate | Nº of Samples Tested | Tensile Strength $X_T^L$ [MPa] | Coefficient of Variation [%] |
|---|---|---|---|
| P1 | 3 | 1555.96 | 7.92 |
| P2 | 5 | 1484.64 | 4.14 |
| P3 | 3 | 1300.12 | 3.47 |
| P4 | 3 | 1190.63 | 4.58 |

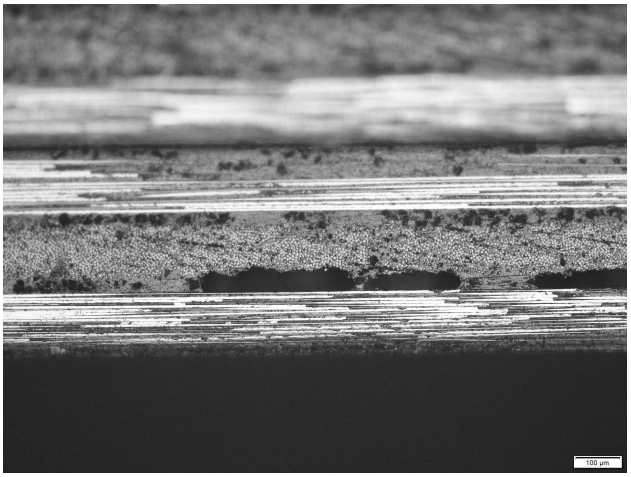


**Figure 4.9:** P1 laminate observed through optical microscopy.

### 4.1.3 Thermoplastic A

For thermoplastic A, the tests of the configurations Q3 and Q4 were performed in the same conditions where the first 3 tests were performed continuously and the last 2 with incremental steps. The graphs obtained from the tests are represented in the figures 4.10 to 4.11. For the Q5 configuration, 8 tests were performed, out of which the first 5 were continuous and the remaining 3 by incremental steps.

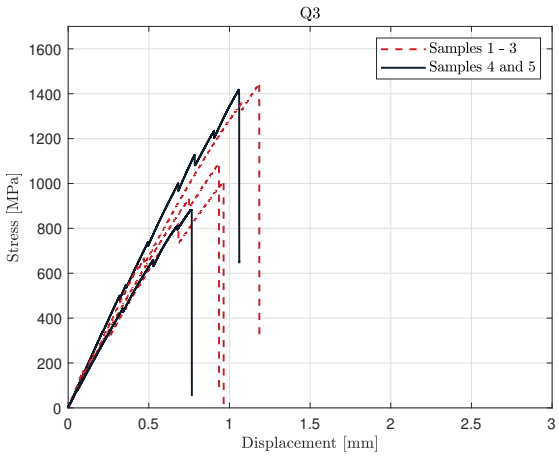


**Figure 4.10:** Stress-displacement tensile test results for configuration with 1 90° ply.

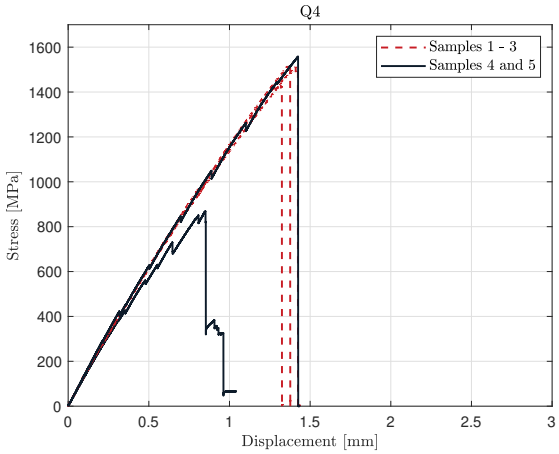


**Figure 4.11:** Stress-displacement tensile test results for configuration with 2 90° ply.

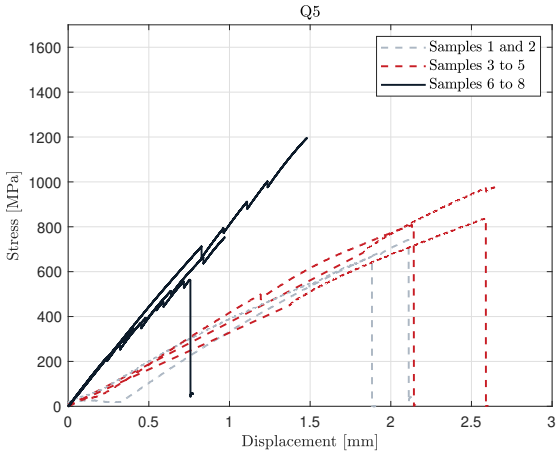


**Figure 4.12:** Stress-displacement tensile test results for configuration with 4 90° ply.

In this material, it was not possible to establish a relationship between ply thickness and the maximum strength of the laminate. It can be observed that the intermediate configuration, Q4, shows a value 21.35% higher than that observed in the thinnest laminate, and 42.34 % higher concerning the thicker laminate. The increasing evolution of tensile strength with decreasing thickness was not observed, which can be justified by poor consolidation of the plates, leading to the formation of in-plane fibre waviness, in the thinnest and thickest laminates, and the value of the intermediate laminate can be considered the most accurate. The different configurations analyzed exhibit a high coefficient of variation due to the dispersion of the results obtained in the tensile tests. This could be related to the low material quality, which may be attributed to the absence of a proper manufacture process.

Fibre waviness can have a downward effect on the mechanical performance of composite laminates and attempts to quantify it are an active area of research [51–55]. The tensile properties of composites decrease with an increase in the magnitude of fibre undulation, which behaves as local shear stress concentrators. The combination of the created interlaminar shear stresses causes premature rupture than failure due to tensile damage for a

specimen with reduced in-plane waviness [55].

**Table 4.3:** Tensile Strength results for the three configuration $[0_2/90_m/0_2]$ of Thermoplastic A.

| Laminate | Nº of Samples Tested | Tensile Strength $X_T^L$ [MPa] | Coefficient of Variation [%] |
|---|---|---|---|
| Q3 | 5 | 1167.66 | 21.51 |
| Q4 | 5 | 1484.64 | 20.95 |
| Q5 | 6 | 856.11 | 24.95 |

### 4.1.4 Thermoplastic B

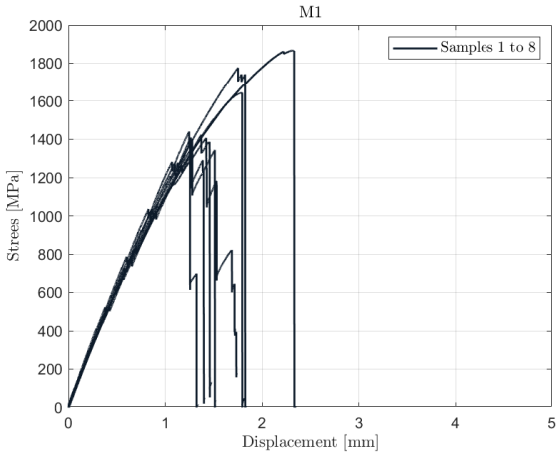


**Figure 4.13:** Stress-displacement tensile test results for configuration with 1 90° ply.

The results obtained from the experimental tests performed for this thermoplastic are shown in figures 4.13 to 4.15. The first three specimens of each configuration were tested continuously while the others were tested with incremental loading. Similarly to the previous materials, the stress-displacement relationship is not completely linear due to the loss of stiffness with the propagation of matrix cracking.

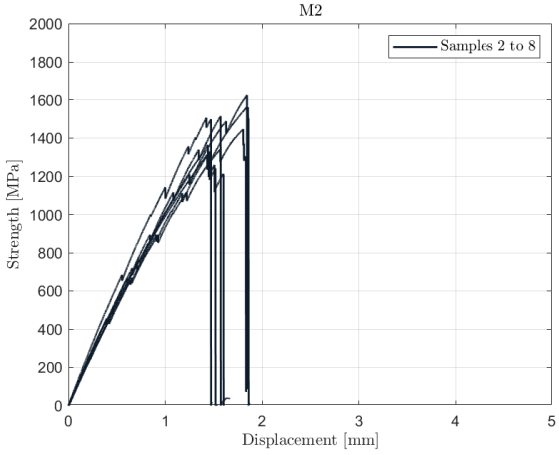


**Figure 4.14:** Stress-displacement tensile test results for configuration with 2 90° plies.

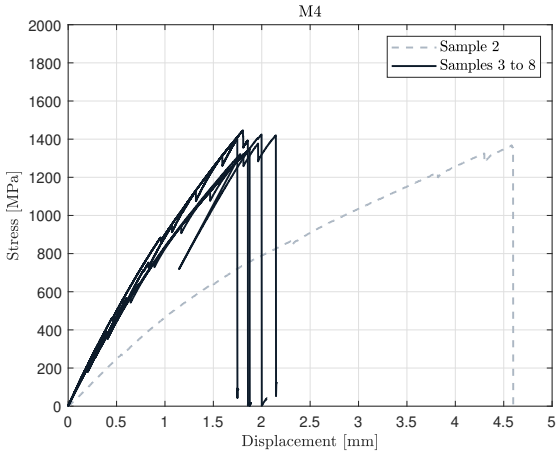


**Figure 4.15:** Stress-displacement tensile test results for configuration with 4 90° plies.

The results of the Tensile Strength of the laminates under study are presented in the following table (Table 4.4). As observed in the results of the other materials, there is a decrease in the maximum tensile strength with the increase in the number of transverse layers in the laminates. In relation to the laminate with only one layer at 90°, there was a decrease of 4.36% in the intermediate configuration and 10.44% in the configuration with more layers.

Compared to the thermoset materials studied, the reduction in tensile strength observed in the different configurations of this thermoplastic is significantly lower. This difference can be attributed to its higher toughness, leading to the proximity of the initial transverse cracking with the final fracture of the material.

**Table 4.4:** Tensile Strength results for the three configuration $[0_3/90_m/0_3]$ of Thermoplastic B.

| Laminate | Nº of Samples Tested | Tensile Strength $X_T^L$ [MPa] | Coefficient of Variation [%] |
|---|---|---|---|
| M1 | 8 | 1545.96 | 12.26 |
| M2 | 7 | 1478.48 | 7.15 |
| M4 | 6 | 1384.58 | 4.18 |

## 4.2 Transverse cracking analysis

In this section, the analysis and comparison of crack initiation and propagation of the different materials are presented. The images were taken during the tensile tests to analyse the initiation of cracks in the transverse layer through specimen loading. From these images, the *in-situ* transverse strength values were obtained for the materials where the appearance of cracks was observed.

The crack growth propagates through the thickness, however, may not extend completely across the width of the specimen. The most representative definition of the damage evolution is given by the ratio between the cracked surface in the volume of the specimen under observation, although, once the propagation extends through the thickness of the specimen, the analysis can be simplified by the ratio between the crack length and the observation of the surface. To simplify the analysis, assuming that the cracks propagate along their width, in the analysis of the obtained results the crack density ($\rho$) was defined by the relation between the number of cracks detected for a certain percentage of the strain (N) and the observation length (L) (Equation 4.1).

$$\rho = N/L \tag{4.1}$$

As mentioned, representative images of the crack formation evolution are presented, with the increase of the applied force, being that the load values will be directly dependent on the material in question, as well as its configuration. Thus, the crack evolution is presented for thermoset A and B and thermoplastic A and B in figures 4.20 to 4.31. The length of observation in each specimen is between 20 and 30 mm.

For some of the laminates studied, the presence of cracks in the matrix was not observed. With the reduction of the number of transverse layers, the appearance of cracks occurs for higher stresses. Thus, in the thinner laminates the cracks occur very close to the maximum failure stress, which makes them difficult to visualize. It should be noted that the resolution of the images obtained makes it rather complicated to visualize the thinner plies, and therefore it is difficult to identify potential cracks.

Finally, it is important to mention that in the next graphical results presented, a characteristic symbol was selected for each configuration of the same material. The variation in the tonality of the curves, with the same symbology, was performed to distinguish different specimens tested with the same configuration and composition. This nomenclature was adopted in order to make the data analysis more understandable.

### 4.2.1 Thermoset A

In thermoset A, for the laminates with only 1 and 3 layers at 90° it is not possible to observe any appearance of cracks. Considering the thickness of the 90° plies is 0.052 mm for one ply and 0.156 mm for 3 plies, a higher resolution than the one used would be necessary to observe the cracks, which could be potentially achieved by utilizing a different

camera lens or reducing the free-length of the samples. For the $[0_6/90_6/0_6]$ laminate the cracks started appearing from 1.15% of strain onward. For the thicker laminates, the cracks are formed from 0.86% of strain. To facilitate the detection of the cracks and increase the contrast, some laminates were white painted on the camera side. The same procedure was performed in the remaining laminates.

The evolution of the crack density as a function of the strain level for the specimens $[0_6/90_{12}/0_6]$ and the $[0_6/90_6/0_6]$ is represented in figure 4.16. It can be observed that crack initiation starts first for the thicker laminate and that its propagation is more sudden initially stabilizing at a lower damage percentage than observed in the thinner laminates.

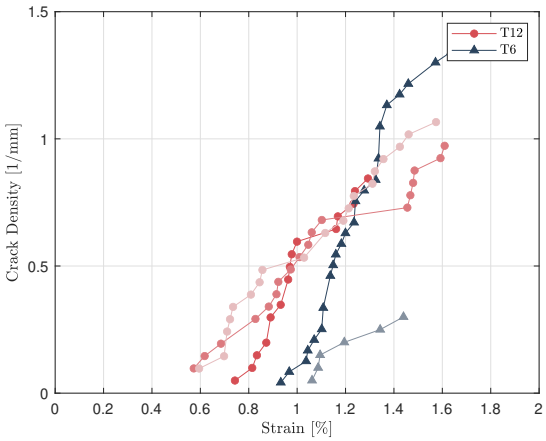


**Figure 4.16:** Crack density evolution in Thermoset A specimens for T6 and T12 laminates.

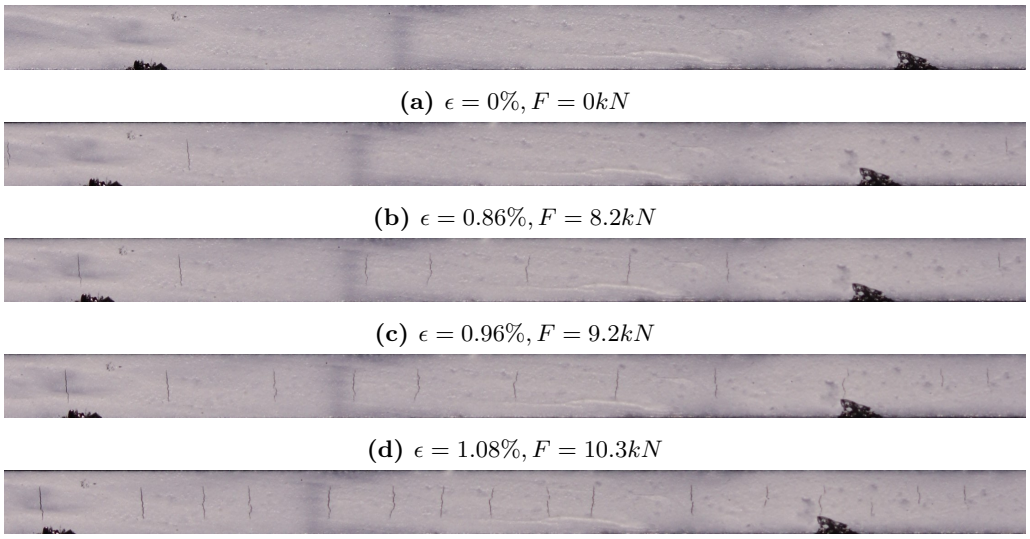

**(a)** $\epsilon = 0\%, F = 0kN$

**(b)** $\epsilon = 0.86\%, F = 8.2kN$

**(c)** $\epsilon = 0.96\%, F = 9.2kN$

**(d)** $\epsilon = 1.08\%, F = 10.3kN$

**(e)** $\epsilon = 1.37\%$, Before Failure

**Figure 4.17:** Example of sequence of images obtained for $[0_6/90_{12}/0_6]$ of Thermoset A (T12).

### 4.2. Transverse cracking analysis

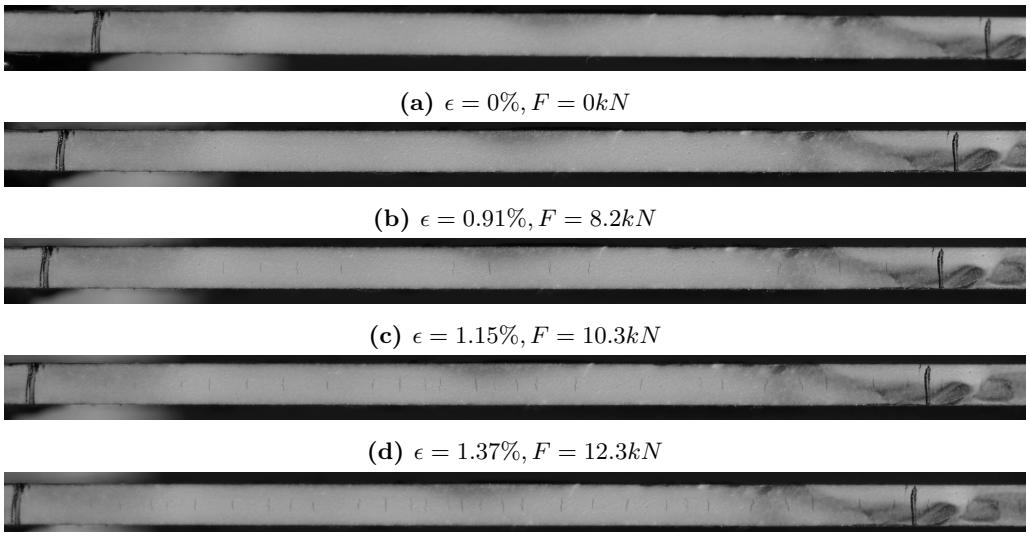

**(a)** $\epsilon = 0\%, F = 0kN$

**(b)** $\epsilon = 0.91\%, F = 8.2kN$

**(c)** $\epsilon = 1.15\%, F = 10.3kN$

**(d)** $\epsilon = 1.37\%, F = 12.3kN$

**(e)** $\epsilon = 1.61\%$, Before Failure

**Figure 4.18:** Example of sequence of images obtained for $[0_6/90_6/0_6]$ of Thermoset A (T6).

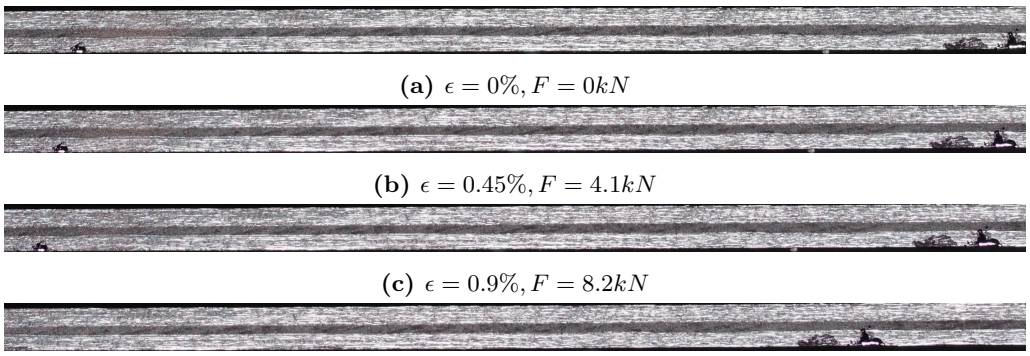

**(a)** $\epsilon = 0\%, F = 0kN$

**(b)** $\epsilon = 0.45\%, F = 4.1kN$

**(c)** $\epsilon = 0.9\%, F = 8.2kN$

**(d)** $\epsilon = 1.49\%$, Before Failure

**Figure 4.19:** Example of sequence of images obtained for $[0_6/90_3/0_6]$ of Thermoset A (T3).

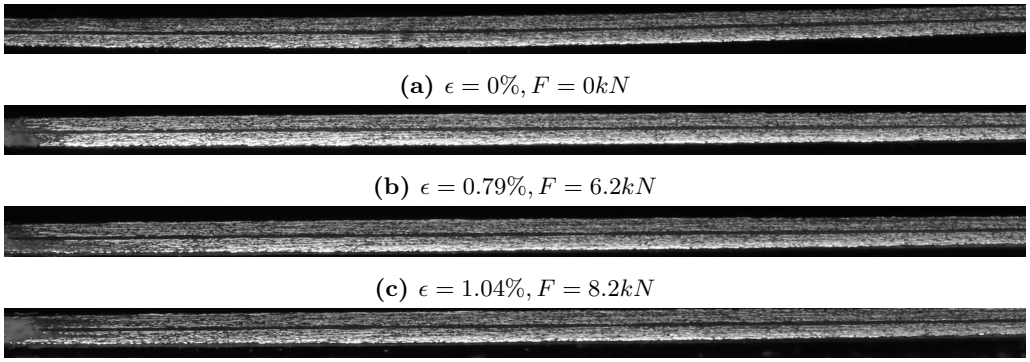

**(a)** $\epsilon = 0\%, F = 0kN$

**(b)** $\epsilon = 0.79\%, F = 6.2kN$

**(c)** $\epsilon = 1.04\%, F = 8.2kN$

**(d)** $\epsilon = 1.68\%$, Before Failure

**Figure 4.20:** Example of sequence of images obtained for $[0_6/90/0_6]$ of Thermoset A (T1).

### 4.2.2 Thermoset B

In the following figures, it is possible to observe the crack initiation and propagation for some specimens with different configurations of the thermoset B laminate. In the laminate with a single transverse ply $[0_2/90_1/0_2]$, delamination was observed at the interface between the layers of different orientations before the final failure of the specimens. After the delamination occurs, the cracks in the transverse layer become visible, as shown in figure 4.24d. Delamination occurred also in the thicker specimens, as mentioned before, but matrix cracking occurs earlier. Regarding the remaining laminates, the transverse cracks appear for a strain percentage of approximately 1.54%, 0.98% and 0.64% for configurations P2, P3 and P4, respectively.

Figure 4.25 presents the crack density growth curves. Similarly to thermoset A, the cracks initiate at lower values of strain with the increase of the transverse layer. With decreasing thickness of the transverse layer, there is a more accelerated and delayed damage growth. In the $[0_2/90_2/0_2]$ laminate, a sudden occurrence of significant damage emerges during the later stages of loading, near the point of ultimate failure. This phenomenon shows the increase of *in-situ* tensile strength as the thickness decreases, leading to a more pronounced escalation in crack density.

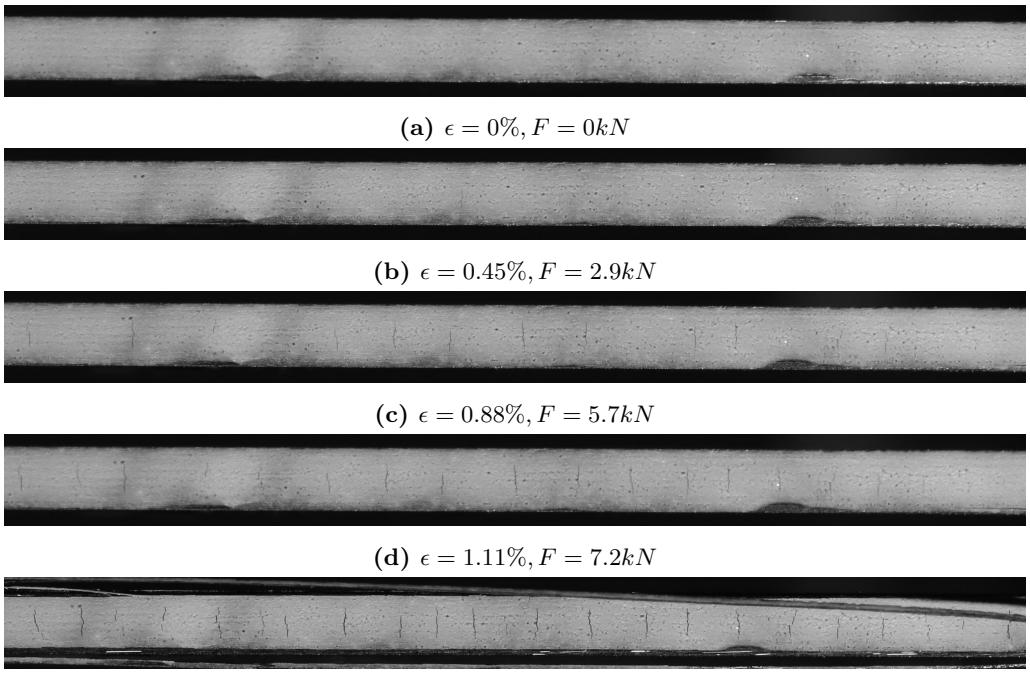

**(a)** $\epsilon = 0\%, F = 0kN$

**(b)** $\epsilon = 0.45\%, F = 2.9kN$

**(c)** $\epsilon = 0.88\%, F = 5.7kN$

**(d)** $\epsilon = 1.11\%, F = 7.2kN$

**(e)** $\epsilon = 2.10\%$, Before Failure

**Figure 4.21:** Example of sequence of images obtained for $[0_2/90_4/0_2]$ of Thermoset B (P4).

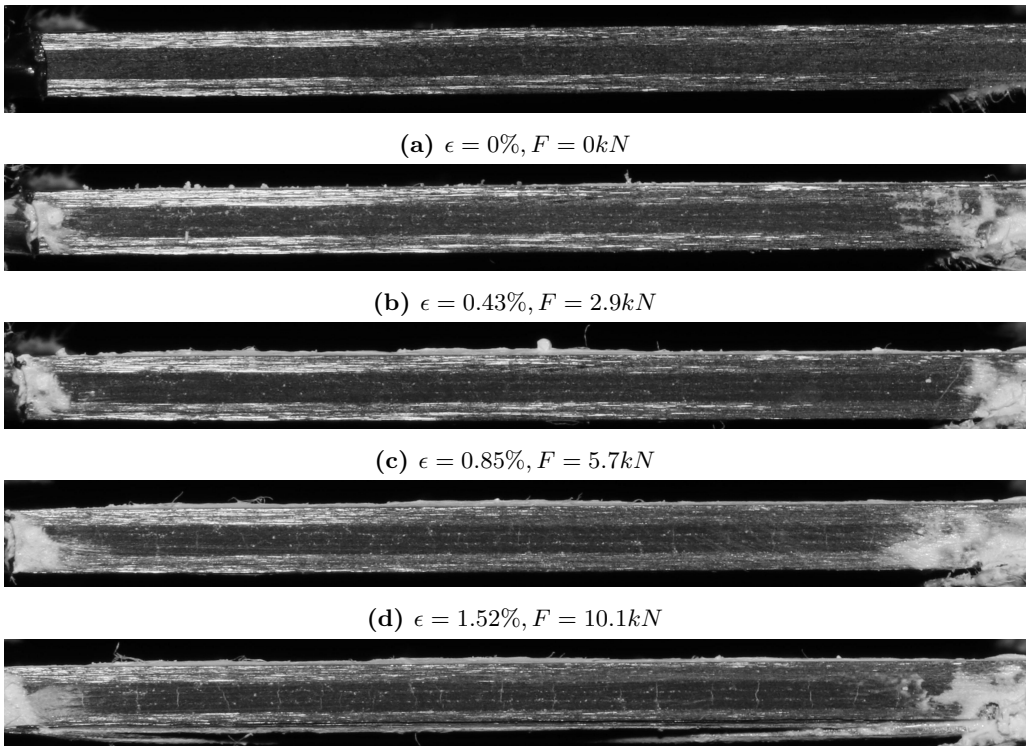

**(a)** $\epsilon = 0\%, F = 0kN$

**(b)** $\epsilon = 0.43\%, F = 2.9kN$

**(c)** $\epsilon = 0.85\%, F = 5.7kN$

**(d)** $\epsilon = 1.52\%, F = 10.1kN$

**(e)** $\epsilon = 1.94\%$, Before Failure

**Figure 4.22:** Example of sequence of images obtained for $[0_2/90_3/0_2]$ of Thermoset B (P3).

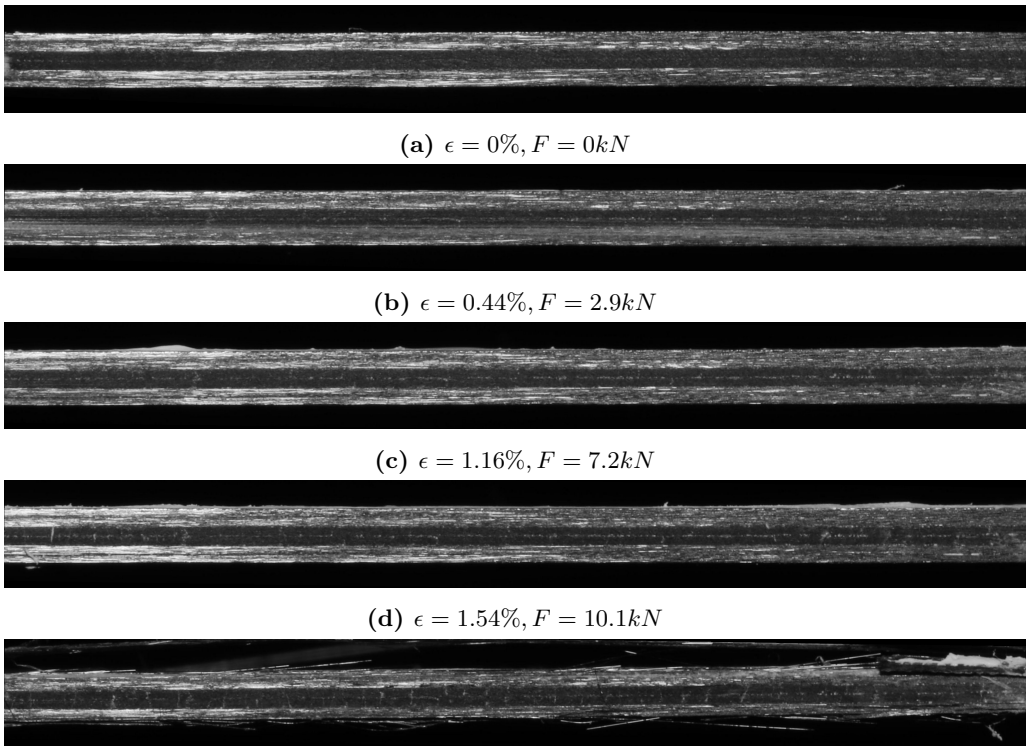

**(a)** $\epsilon = 0\%, F = 0kN$

**(b)** $\epsilon = 0.44\%, F = 2.9kN$

**(c)** $\epsilon = 1.16\%, F = 7.2kN$

**(d)** $\epsilon = 1.54\%, F = 10.1kN$

**(e)** $\epsilon = 2.00\%$, Before Failure

**Figure 4.23:** Example of sequence of images obtained for $[0_2/90_2/0_2]$ of Thermoset B (P2).

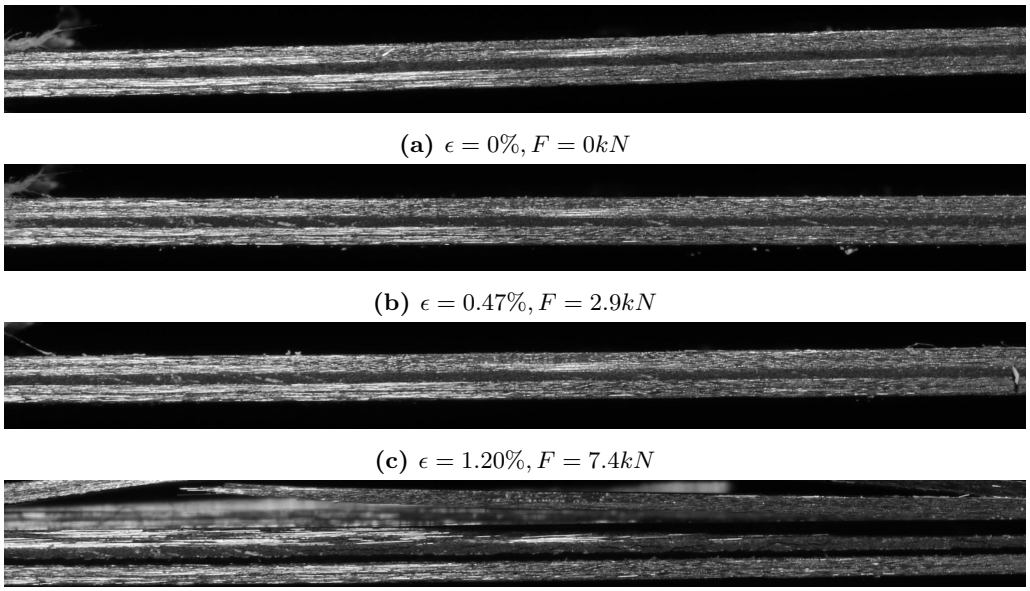

**(a)** $\epsilon = 0\%, F = 0kN$

**(b)** $\epsilon = 0.47\%, F = 2.9kN$

**(c)** $\epsilon = 1.20\%, F = 7.4kN$

**(d)** $\epsilon = 1.84\%$, Before Failure

**Figure 4.24:** Example of sequence of images obtained for $[0_2/90/0_2]$ of Thermoset B (P1).

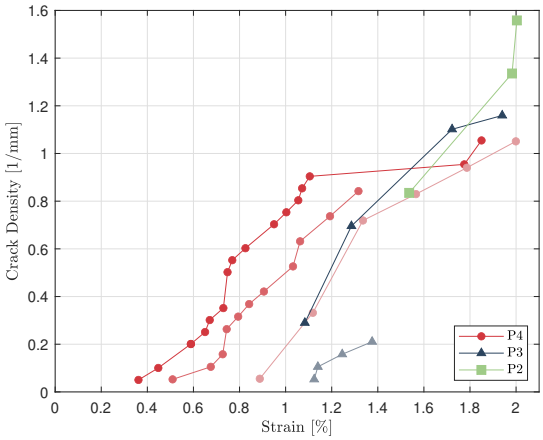


**Figure 4.25:** Crack density evolution in Thermoset B specimens for P2, P3 and P4 laminates.

### 4.2.3 Thermoplastic A

Compared with thermoset composites, the Thermoplastic A system showed the nucleation of the first transverse crack at a lower level of strain. For the laminate $[0_2/90_4/0_2]$, in fact, the appearance of cracks was observed at 0.3% strain, while for the laminate $[0_2/90_2/0_2]$ cracks were only observed at 0.6%. In the thinner laminates, no cracks were spotted during the tests. In the damage evolution observed for the laminate Q5, it can be seen the formation of cracks concentrated on the left side of the image, where the aforementioned fibre waviness defect is located.

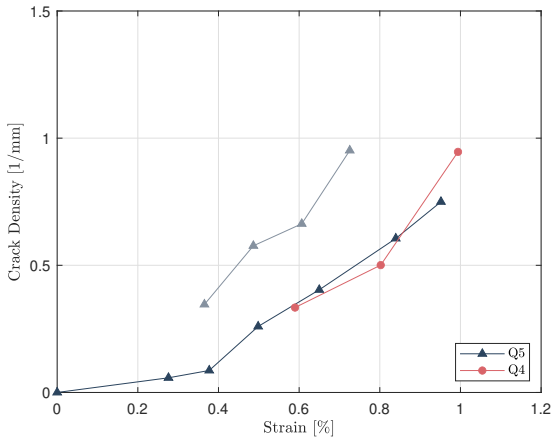


**Figure 4.26:** Crack density evolution in Thermoplastic A specimens for Q4 and Q5 laminates.

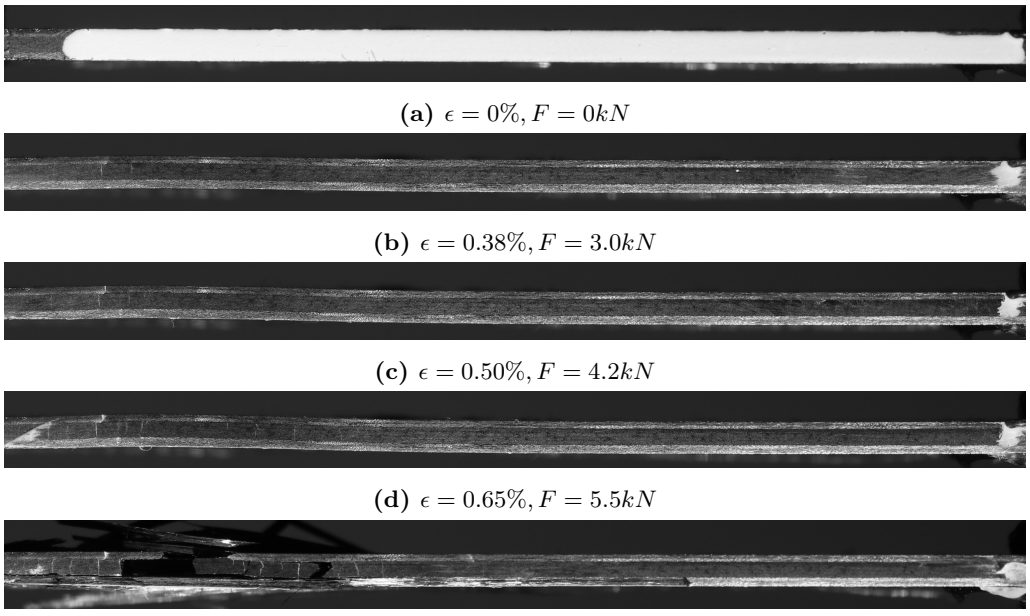

**(a)** $\epsilon = 0\%, F = 0kN$

**(b)** $\epsilon = 0.38\%, F = 3.0kN$

**(c)** $\epsilon = 0.50\%, F = 4.2kN$

**(d)** $\epsilon = 0.65\%, F = 5.5kN$

**(e)** $\epsilon = 0.95\%$, Failure

**Figure 4.27:** Example of sequence of images obtained for $[0_2/90_4/0_2]$ of Thermoplastic A (Q5).

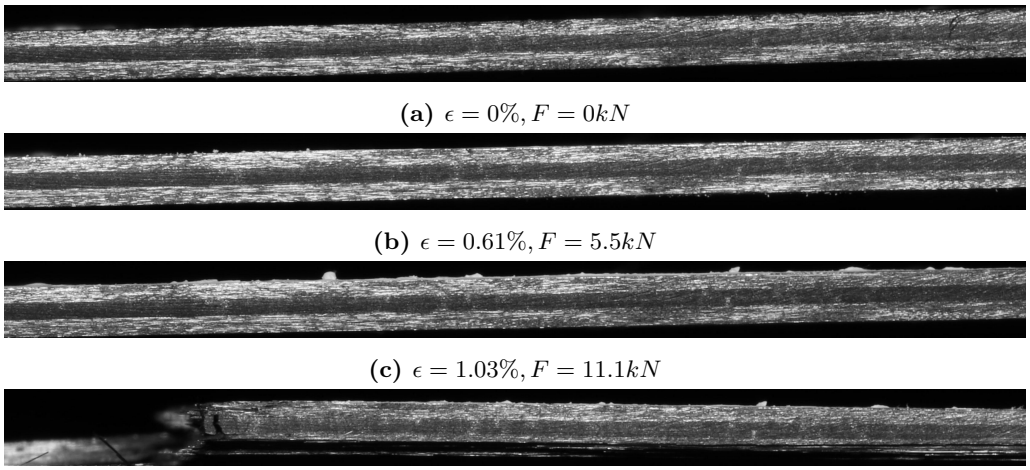

**(a)** $\epsilon = 0\%, F = 0kN$

**(b)** $\epsilon = 0.61\%, F = 5.5kN$

**(c)** $\epsilon = 1.03\%, F = 11.1kN$

**(d)** $\epsilon = 1.53\%$, Failure

**Figure 4.28:** Example of sequence of images obtained for $[0_2/90_2/0_2]$ of Thermoplastic A (Q4).

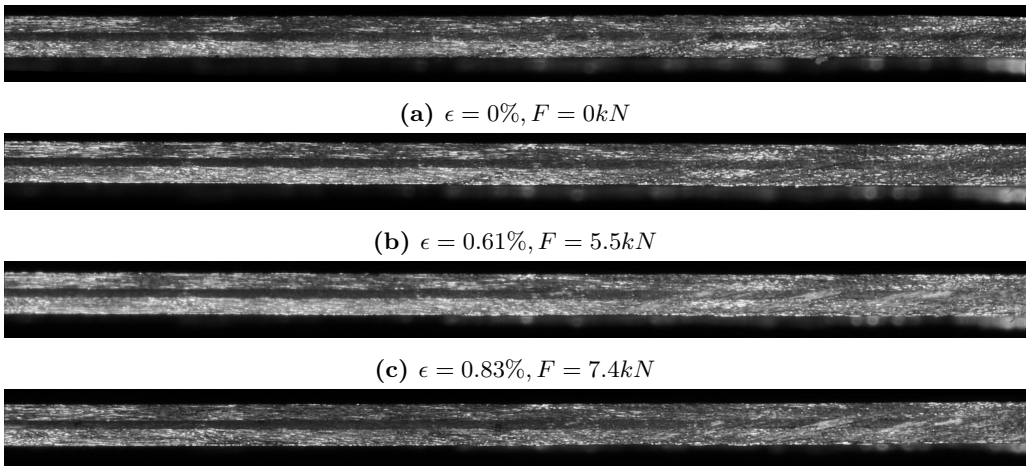

**(a)** $\epsilon = 0\%, F = 0kN$

**(b)** $\epsilon = 0.61\%, F = 5.5kN$

**(c)** $\epsilon = 0.83\%, F = 7.4kN$

**(d)** $\epsilon = 1.17\%$, Before Failure

**Figure 4.29:** Example of sequence of images obtained for $[0_2/90/0_2]$ of Thermoplastic A (Q3).

### 4.2.4 Thermoplastic B

As observed for some of the specimens previously analysed, in the laminates of configuration $[0_3/90/0_3]$ and $[0_3/90_2/0_3]$ the existence of transversal cracking only becomes visible after delamination at the interface $0°/90°$. Due to the high toughness of the thermoplastic materials interfaces, the appearance of transverse cracks was delayed until delamination occurred and is evident in sub-figures 4.32e and 4.33d. In the case of the M2 laminate, small cracks are observed that do not propagate through the entire thickness of the ply instead, stopped at the interface between the two transverse layers.

For the laminate with a thicker configuration, the appearance of some cracks was observed close to 0.82% strain. Despite the low number of data points obtained for this analysis, it is possible to observe a growth in crack density until the final failure of the M4 laminate, similar to what was observed in the other materials.

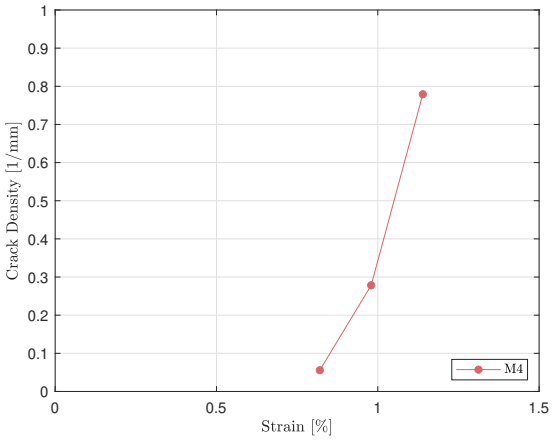


**Figure 4.30:** Crack density evolution in Thermoplastic B specimens for M4 laminate.

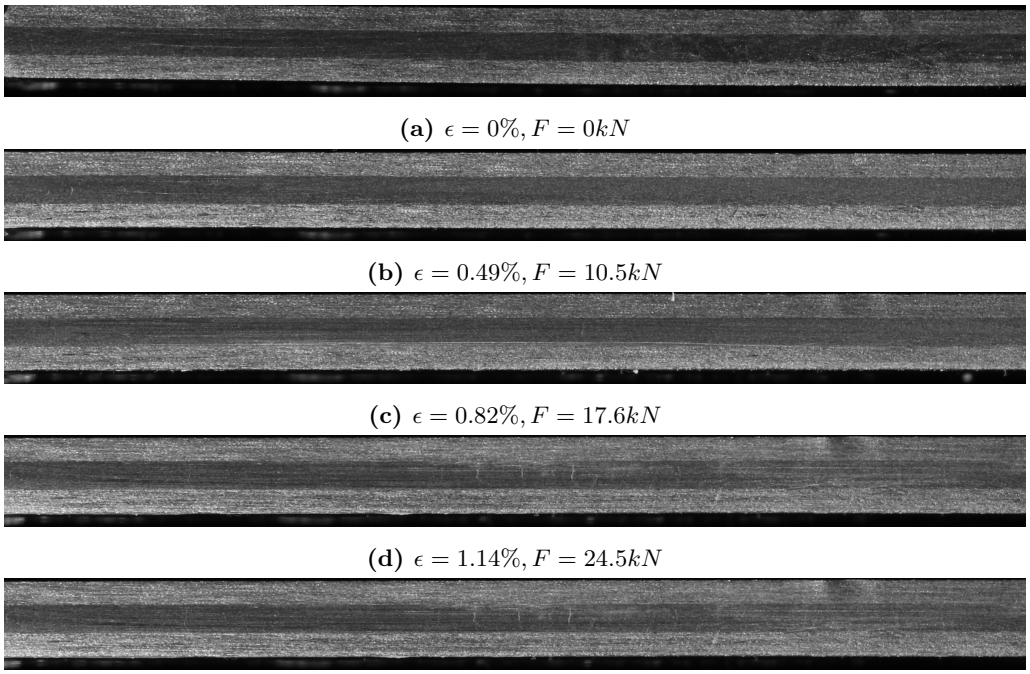

**(a)** $\epsilon = 0\%, F = 0kN$

**(b)** $\epsilon = 0.49\%, F = 10.5kN$

**(c)** $\epsilon = 0.82\%, F = 17.6kN$

**(d)** $\epsilon = 1.14\%, F = 24.5kN$

**(e)** $\epsilon = 1.22\%$, Before Failure

**Figure 4.31:** Example of sequence of images obtained for $[0_2/90_4/0_2]$ of Thermoplastic B (M4).

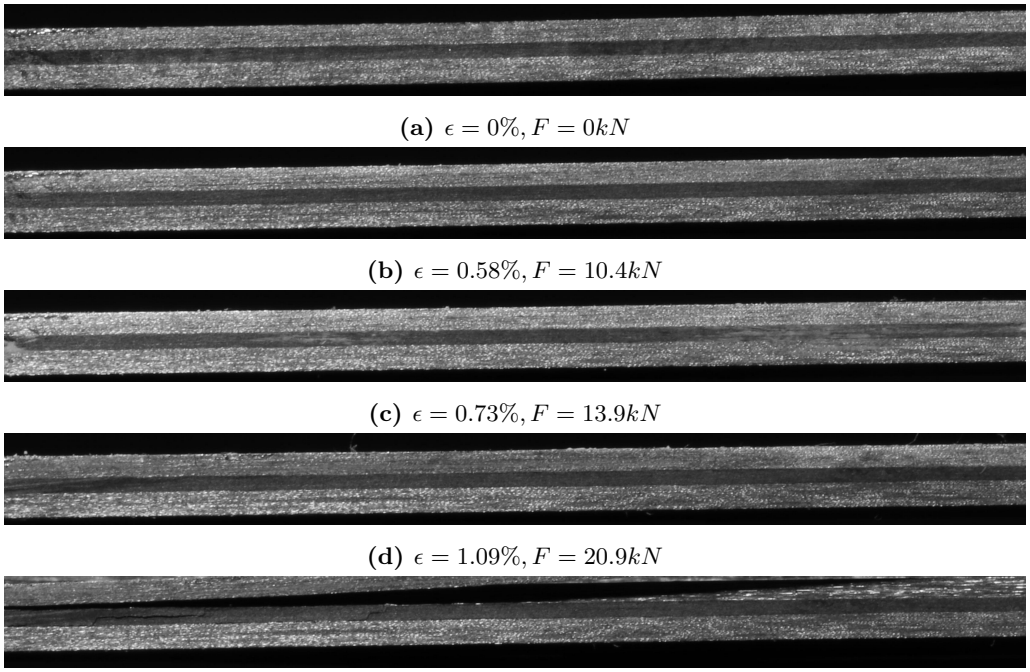

**(a)** $\epsilon = 0\%, F = 0kN$

**(b)** $\epsilon = 0.58\%, F = 10.4kN$

**(c)** $\epsilon = 0.73\%, F = 13.9kN$

**(d)** $\epsilon = 1.09\%, F = 20.9kN$

**(e)** $\epsilon = 1.18\%$, Before Failure

**Figure 4.32:** Example of sequence of images obtained for $[0_3/90_2/0_3]$ of Thermoplastic B (M2).

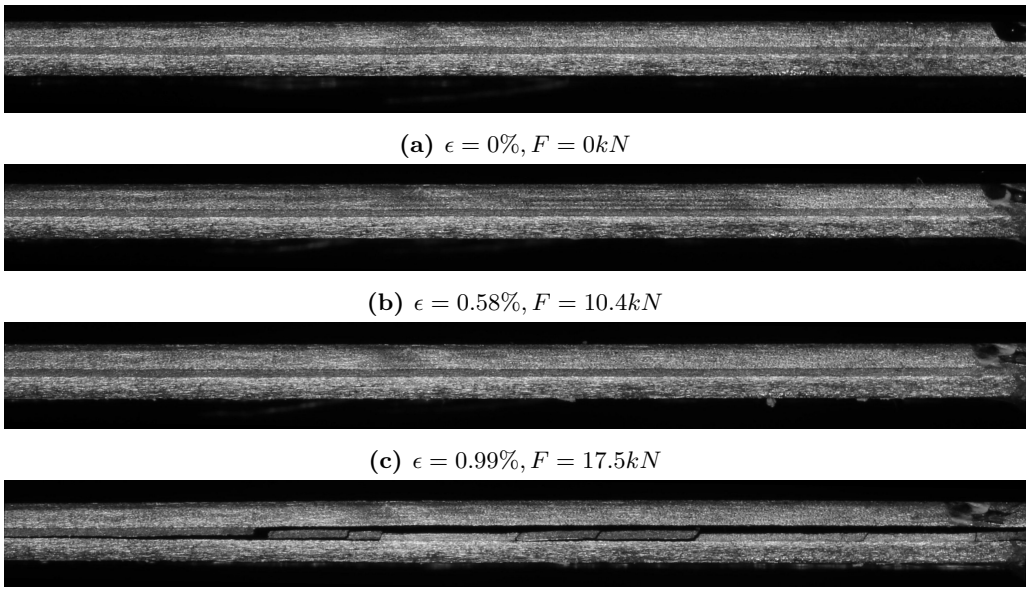

**(a)** $\epsilon = 0\%, F = 0kN$

**(b)** $\epsilon = 0.58\%, F = 10.4kN$

**(c)** $\epsilon = 0.99\%, F = 17.5kN$

**(d)** $\epsilon = 1.01\%$, Before Failure

**Figure 4.33:** Example of sequence of images obtained for $[0_3/90/0_3]$ of Thermoplastic B (M1).

### 4.2.5 Comparation

A comparison between laminates of the same thickness was made to establish the influence of the type of material on the obtained results. By analysing the crack density evolution in the two thicker thermoset laminates (Figure 4.34a), it is observed that the crack initiation occurs in the same range of strain values and reaches a similar damage percentage. In Figure 4.34b, the distinct behaviour of the thermoplastic is easily identifiable, observing the premature onset of the cracks. There can also be detected a more sudden crack density growth in the thermoset material.

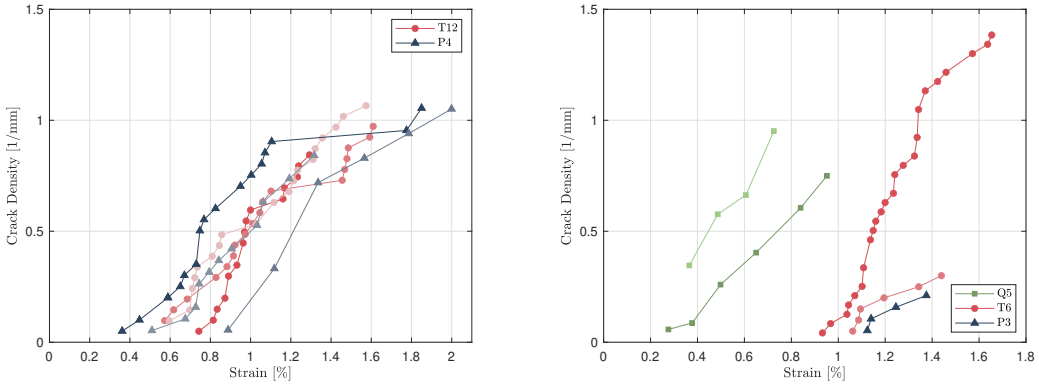


**(a)** Thermoset A and Thermoset B **(b)** Thermoplastic A, Thermoset A and B

**Figure 4.34:** Comparison of the behaviour of laminates of the same thickness of different materials.

As previously mentioned, the specimens used in the tensile tests of thermoplastic A had manufacturing defects, which could influence the results obtained by anticipating the

initiation of cracks in the matrix. For a more accurate analysis, it would be pertinent to carry out further experimental tests, nevertheless, this comparison might be a useful starting point to speculate a distinct behaviour between thermoplastic and thermoset materials.

### 4.2.6 Crack Spacing

The crack spacing measurement was performed using the Fiji ImageJ measurement tool and the average spacing was determined as a function of percentage strain for each of the specimens where cracks could be identified. The evolution of the average crack spacing as a function of the percentage strain is shown in figure 4.35.

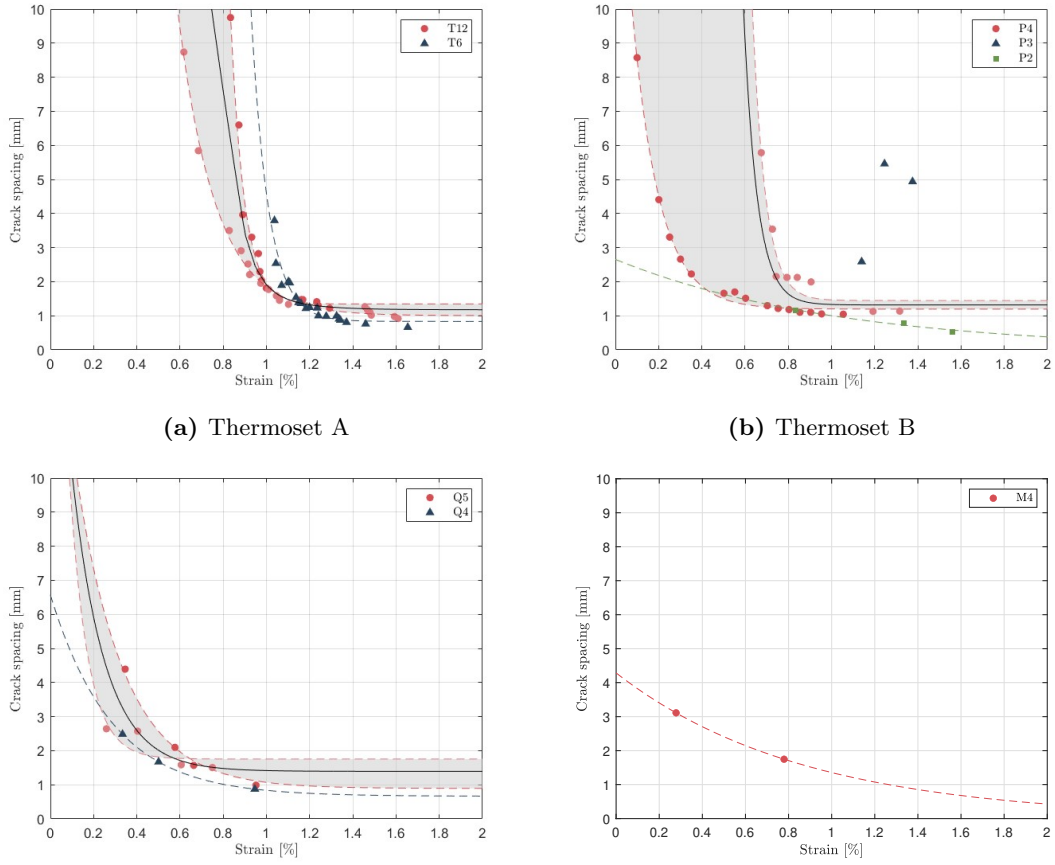


**(a)** Thermoset A

**(b)** Thermoset B

**(c)** Thermoplastic A

**(d)** Thermoplastic B

**Figure 4.35:** Average crack spacing as a function of % Strain.

Analyzing the graphs presented for each material under study, it can be observed a decrease in the spacing between cracks with the percentage strain increase. The spacing between cracks for lower values of strain is non-uniform, tending to a homogeneous distribution for high values of strain.

Analysing the evolution of the average spacing for the thermoset A specimens, it is possible to clearly verify that the decrease occurs in a similar way for the configurations

with different numbers of transversal layers. The spacing settles down to a value of approximately 1 mm. A similar relationship can be observed for the configurations with four and two transverse layers in thermosetting B, where the average spacing between gaps converges is also about 1 mm. The data obtained from the specimen with three transverse layers of specimen P3 did not allow the detection of the formation of many cracks, thus hindering any trend towards the crack spacing distribution.

Regarding the analysis of thermoplastic A, despite the low number of cracks observed, there is a decrease in the average crack spacing without being possible to reach a stagnation point. In the analysis of thermoplastic B, given the lack of information, the results obtained are not significant.

The evolution of the distance between cracks for the different configurations of each material shows practically equal behaviour, stabilising at a similar value and going from an exponential decrease to a constant average value, as plotted with the fit curves.

In Table 4.5 can be found the parameters that allowed the construction of these adjustment curves, based on the equation 4.2. For configurations with multiple curves, such as the T12, P4, and Q5 laminates, average curves were generated by fitting the individual test curves.

$$y = ae^{-bx} + c \tag{4.2}$$

**Table 4.5:** Parameters for the adjustment equations for the different materials and correlation coefficient.

| **-** | **T12** | **T6** | **P4** | **P2** | **Q5** | **Q4** |
|---|---|---|---|---|---|---|
| a | 5.64E+02 | 9.67E+05 | 1.07E+05 | 2.65E+00 | 1.70E+01 | 5.91E+00 |
| b | 5.705 | 12.46 | 15.88 | 0.9738 | 6.62 | 3.526 |
| c | 0.9347 | 0.8336 | 1.317 | 0 | 1.393 | 0.6618 |
| $R^2$ | 0.9845 | 0.9075 | 0.9987 | 0.9654 | 0.9977 | 1 |

It can be observed that, globally, the correlation coefficient between these two variables is considerably high, with the minimum value obtained being 0.9075, which can be translated into an almost ideal fit for all the materials studied.

After a detailed literature review on this correlation, it was not possible to find any theoretical or even experimental model that correlated these two variables. Thus, it is considered relevant, for future studies, a deeper study of this relationship to develop theoretical models that allow a more accurate prediction for crack spacing evolution for thermoplastics and thermosets materials.

# Chapter 5

# Synchrotron Radiation Computed Tomography Analysis

In recent years, there has been significant growth in the availability of powerful imaging tools such as digital image correlation, thermography, radiography and computed tomography, which can provide detailed information of material morphology and elucidate on damage formation and propagation. In the context of the study of failure mechanisms in composite materials, digital image correlation, which allows real-time visualization of damage on the specimen surface, has been the most commonly used. However, this technique only provides surface information and, due to the complexity of the failure mechanisms of composite materials may not fully elucidate on the internal behaviour of the material. Therefore, more recently, three-dimensional (3D) observations based on computed tomography have been used to better under- stand the failure mechanisms in composite materials. Of these methods, synchrotron radiation computer tomography stands out as the most informative CT method given that it uses synchrotron radiation as the X-ray source, allowing for higher resolution and 100x faster scan times compared to traditional laboratory computed tomography techniques [51, 52]. This allows, not only the 3D visualization of damage profiles for a single load, but opens the possibility of analysing damage evolution as a function of the applied load. These tests are called [56, 57] Synchrotron Radiation Computed Tomography Analysis.

In this chapter, the study of the ply thickness effect on the initiation and propagation of transverse cracking in thermoplastic A material is studied in more detail, through the analysis of *in-situ* double-edge notched tensile tests imaged using synchrotron radiation computed tomography (SRCT). The details of the study are reported hereafter.

## 5.1 *In-Situ* DENT Testing via SRCT

In-situ synchrotron radiation computer tomography testing consists on performing computed tomography imaging while a sample is being loaded in a synchrotron radiation facility. This implies, the use of a testing machine that can be mounted on a rotating stage

and load a sample to different load percentages, allowing imaging of the sample at that load level. Generally, these tests are done as follows:

- A sample is loaded in the testing machine and loaded to 5N (so that it does not move) and the interest zone is located and scanned using SRCT.
- Then, the sample is loaded to a given load, and scanned again in the interest zone.
- The process is repeated until the sample brakes, allowing the visualization of crack formation and propagation as a function of the load.

Here, the technique was used to investigate the onset and propagation of matrix cracks in $90^{o}$ plies as a function of the ply thickness for Thermoplastic A, whose mechanical properties were shown and discussed in Chapter 3. Tasks 5.1.1, 5.1.2 and 5.1.3 were performed by colleagues of the group, but are summarized here for the sake of completeness. This thesis contribution lies in the image analysis reported in section 5.2.

### 5.1.1 Sample Preparation

For this analysis cross-ply laminates with the three previously analysed stack sequences, Q3 - $[0_2/90_1/0_2]$, Q4 - $[0_2/90_2/0_2]$ and Q5 - $[0_2/90_4/0_2]$, were considered. Specimens with 4 mm wide, 100 mm long double-edge notched tension (DENT) with two 1.25 mm radius edge notches centred lengthwise were used. This specimen geometry was chosen to ensure: an ultimate load lower than 5kN (maximum load of the testing machine) and that the damage would be localized in a known area (the notches) for imaging purposes. The samples were cut from the plates using CNC machine.

Given the configuration of the testing machine grips to be used in the SRCT facility, the samples were tabbed using T-shaped steel tabs. To guarantee the alignment and quicken the tabbing process, a tabbing rig shown in Figure 5.1a was used. The tabbing process can be divided into the following steps:

- Preparation of the bonding surface of the specimen using sandpaper to improve the adhesion of the adhesive to the tabs and the specimen.
- Preparation of the tabbing rig starting with the application of release agent on the alignment pins and on the bolts of the alignment rig and doing the placement of two layers of Teflon on the tab plates, to guarantee the correct demolding.
- Preparation of the adhesive and application of the same on the polished surface of the specimens.
- Proper positioning of the previously cut metallic tab plates and the specimens between two metal support plates to finish the assembly of the mould.
- The adhesive was cured with a 24 hour cycle at room temperature followed by 1 hour in an oven at 80°C. After the cure, the tabbed specimens were cut from the support plates.

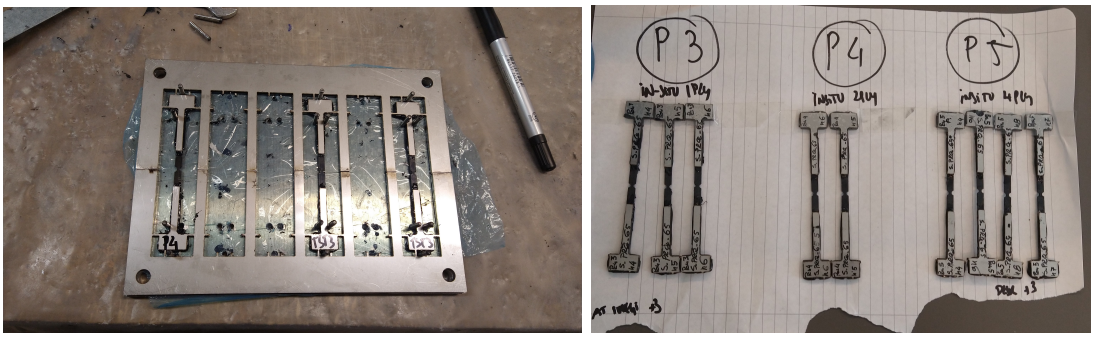


**(a)** **(b)**

**Figure 5.1:** a) Specimens and the tab support plates positioning in the tabbing rig; b) Specimen prepared.

### 5.1.2 *Ex-situ* Tests

First, to establish the load steps of interest to be analyzed using SRCT, the samples were tested *ex-situ*. The samples were tested in an Instron 5900R Universal Testing Machine using a 200 kN load cell, and a camera was used to analyze the surface edge of the sample and detect crack formation as explained in Chapter 3. These preliminary tests allowed the determination of the failure load of the 3 configurations. By making use of the load and geometry, the ultimate strength (Table 5.1) and strain were determined.

**Table 5.1:** Tensile Strength results for the four configuration $[0_2/90_m/0_2]$ of Thermoplastic A

| Laminate | Nº of Samples Tested | Maximum Load [N] | Tensile Strength $X_T^L$ [MPa] |
|---|---|---|---|
| Q3 | 2 | 1823.00 ± 96.22 | 579.73 ± 12.72 |
| Q4 | 3 | 2098.33 ± 75.93 | 602.98 ± 13.74 |
| Q5 | 2 | 1763.00 ± 61.00 | 411.24 ± 15.03 |

Through the tensile tests previously performed the maximum force value was established as 2098 N. From these values a maximum value of the stress in the $0^{\circ}$ plies was obtained (by dividing the load by the width and thickness of the $0^{\circ}$ plies) and of the ultimate strain (dividing by the Young's modulus of the $0^{\circ}$ ply). This strain value of 0.66 % was used as a reference for all configurations in the in-situ tests and used to define similar stopping points in each of the tests.

### 5.1.3 *In situ* Tests

The in-situ DENT tests were carried out in 47XU beamline at the Super Photon ring-8 GeV (SPring-8), located in Hyogo, Japan. The setup of the experimental tests is shown in Figure 5.2. One sample per configuration was tested under displacement control at a rate of 0.3 mm/min, and scanned at 6 strain levels: 0% (before loading), 0.2%, 0.3%, 0.4% and 0.5 % of strain, which were established based on *ex-situ* tests. The load corresponding to each strain was computed for each sample. The samples were loaded, and when reached the intended value, were unloaded to 90% of that load before scanning to speed up the stress relaxation process.

At each strain level, three scans per sample in three adjacent locations near one of the notches were made: P1, P2 and P3. To perform a scan, the sample is rotated 180°, it is stopped 1800 times during that period (1800 projections) and a 2D X-ray is taken (28 KeV X-ray energy, 80 ms exposure, 0.5 µm isotropic voxel size). After all the scans are taken, the 3D image is reconstructed, resulting in a volume composed of a sequence of 2D slices. The detector size was 2048x2048 pixels, resulting in a scan field of view of 1.024 x 1.024 $mm^2$.

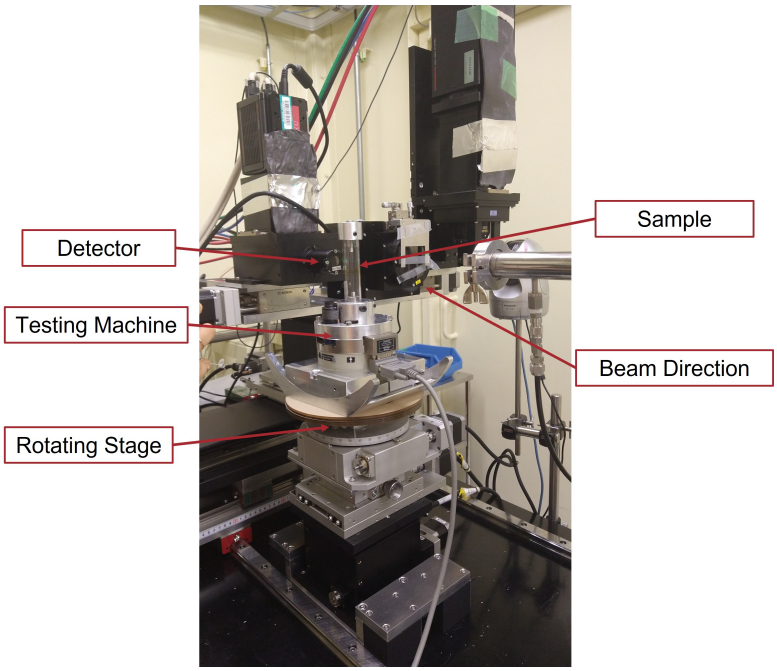


**Figure 5.2:** Experimental Test Setup for *in-situ* DENT tests.

## 5.2 Image Process and Segmentation

Data analysis was performed using the Fiji ImageJ program. The analysis required for each sample and load step:

- Volume rotation: The obtained data is composed of a stack of 2D images, where the stack direction is the loading (0°) direction. This means that the motive of interest, the cracks in the 90° plies along the length of the sample are not visible in the original images. For this reason, the first step consisted of rotating the image stacks of each scan to the layer orientation at 90°, using the reslice stack tool of ImageJ (Figure 5.3b).
- Stitching of the 3 adjacent scans: To obtain the full scan visualisation the 3 capture adjacent scans were combined into one volume as shown in figure 5.3c. For this step, the combine stacks tool was used, after cropping the overlapped image section.
- Cropping: Given the focus in the region of the layers at 90° the images were cropped by the region of interest, removing the scanned air and 0° plies (highlighted in the yellow box of the figure 5.3c).

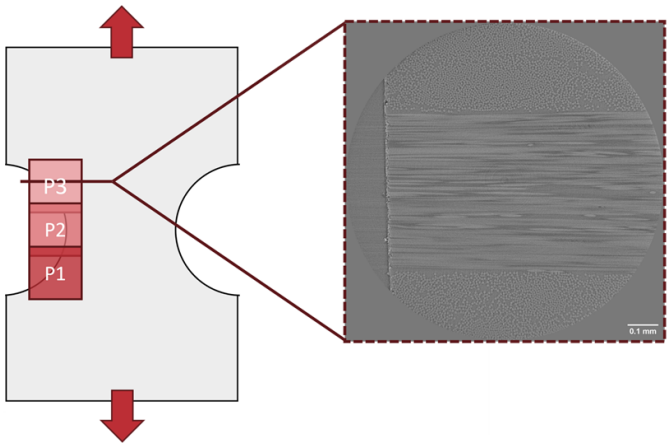


**(a)** Representation of the visualization section divided into the three scanning segments.

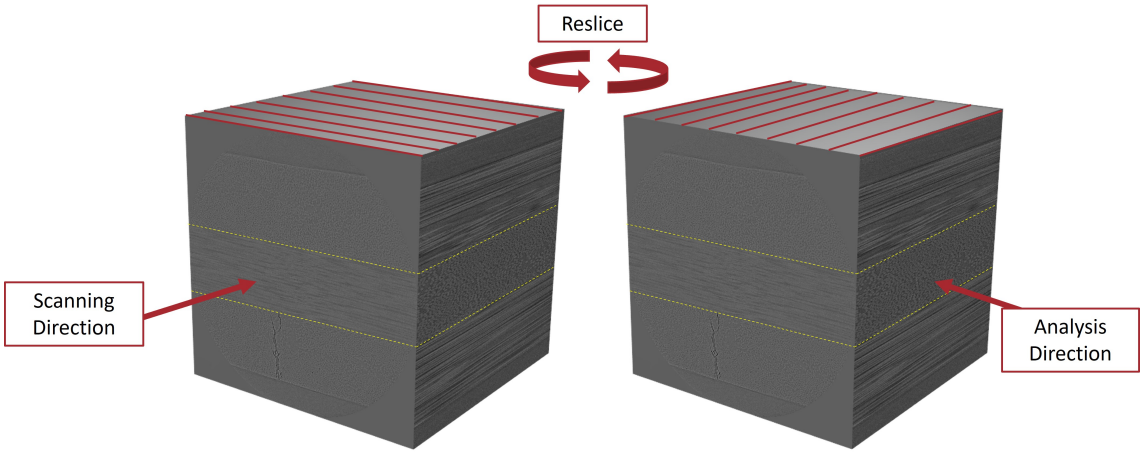


**(b)** Representation of the Reslice of the stack volume.

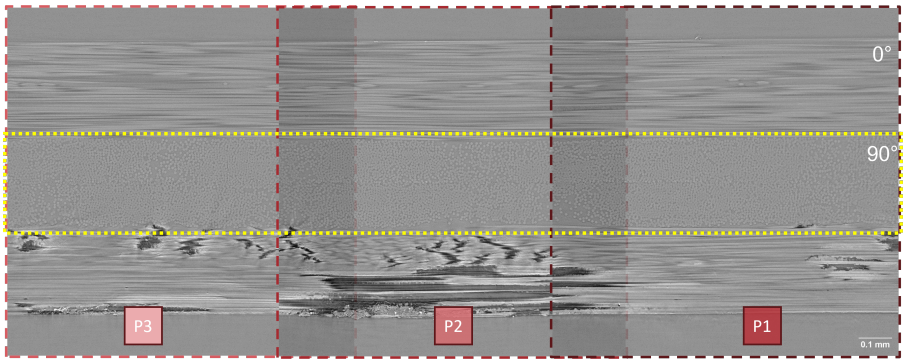


**(c)** Combination of the three segments of the scan after volume rotation with the crop region highlighted in yellow.

**Figure 5.3:** Post-processing used to define the damaged volume.

Following these 3 steps, the volumes were ready to be segmented. The image segmentation was performed using:

- Image adjustment: Using the automatic adjustment tool, the brightness and contrast of the image stack were adjusted, allowing for the differentiation between the different constituents (matrix, fibres, and blanks corresponding to the absence of material or cracks). To reduce image noise and fine details, a Gaussian blur filter was applied, which resulted in the blending of the boundaries between the matrix and the fibres.
- Image conversion: The image is converted using a binary mask to separate the regions of interest (ROI). For this step, the maximum entropy threshold was chosen (Figure 5.4b).

With the stack converted into a binary mask, the reconstruction of the damaged volume was performed using the 3D viewer window from the software. It should be noted that the method used for this analysis does not present the greatest accuracy, since it is an automatic method without an appropriate adjustment to the intended demand.

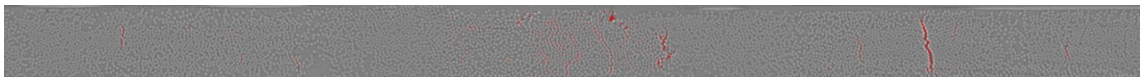

**(a)** Image obtained after joining segments and cut by the region of the transversal ply.

**(b)** Image after removing outliers and apply the Binary Mask.

**Figure 5.4:** Post-processing used to define the damaged volume.

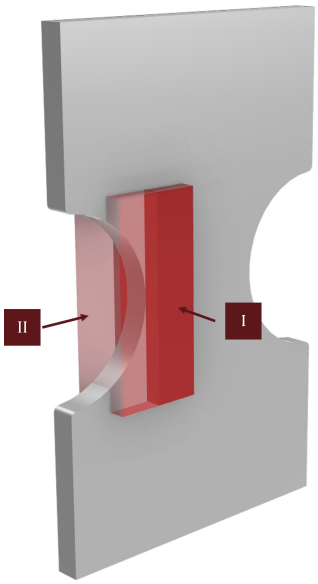


**Figure 5.5:** Representation of the DENT specimen with a region of interest observed during the in situ SRCT, light pink, and the analysed region, dark pink.

The *in-situ* mechanical tests were realized for one specimen of each of the configurations under study. With the images captured for each load step, the damage state volumes were defined focusing the analysis on one side of the specimen in the beforementioned area. To facilitate the reconstruction of the damaged volume, the area of analysis that encompassed the notch was disregarded, decreasing the volume of analysis for the remaining internal section of the specimen. As previously mentioned, the tomograms obtained in the tests are oriented perpendicularly to the 0° layers. As the objective is to analyse the damage in the transversal matrix, the segmentation for a perpendicular plane to the 90° layers was performed. The volume and the views used for the analysis are shown in the scheme in figure 5.5.

## 5.3 Analysis

The data obtained in the double-edge notched tension tests via the synchrotron radiation computed tomography for load steps for strain percentages of 0, 0.2, 0.3, 0.4 and 0.5 are presented in this section for laminates with one, two and four transversal plies of the thermoplastic A. These results were obtained with the aim to analyse the damage caused by matrix cracks in the transverse layers of thermoplastic-based composite through a 3D analysis.

The damage state at each loading step was quantified by calculating the surface area of the matrix damage in each image, and consequently calculating the volume associated with that area. In order to simplify the analysis, the damage volume was quantified as a percentage of damage, by considering the fractured volume as a function of the total volume analysed.

In figures 5.7 to 5.12 it is shown the top (the view I represented in figure 5.5) and front view (the view II represented in figure 5.5) of the damage volumes for each load step in the different specimens analysed. The volume corresponding to the transverse cracks formed is shown in red for the Q3 configuration, in light blue for the Q4 configuration and in dark blue for the Q5 configuration.

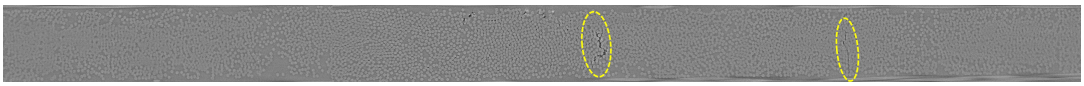

**(a)** Captured image for an unload specimen Q3.

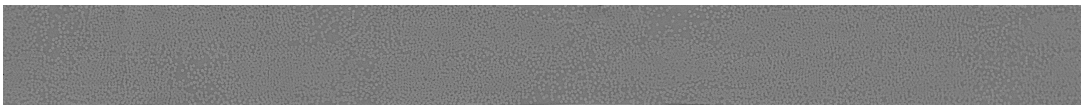

**(b)** Captured image for an unload specimen Q4.

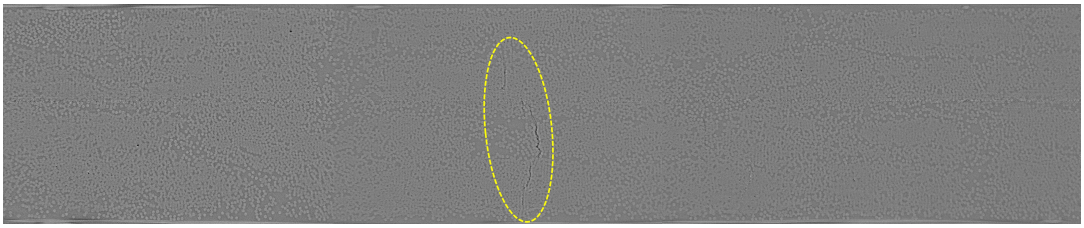

**(c)** Captured image for an unload specimen Q5.

**Figure 5.6:** Captured images of the inner region of the specimen after the notch.

In the first step, in the unloaded specimen, it is possible to see some percentage of damage for the laminates Q3 and Q5, that can be justified by the post-processing methods used or by the existence of manufacturing defects. By examining the region after the notch in the three configurations (Figure 5.6), some damage is observed in the central zone of the Q3 and Q5 laminates (highlighted in figures 5.6a and 5.6b). The presence of these premature cracks may be attributed to the induction of high-stress gradients caused by the notched edge. Additionally, a smaller second crack can be observed in the Q3 laminate (Figure 5.6a).

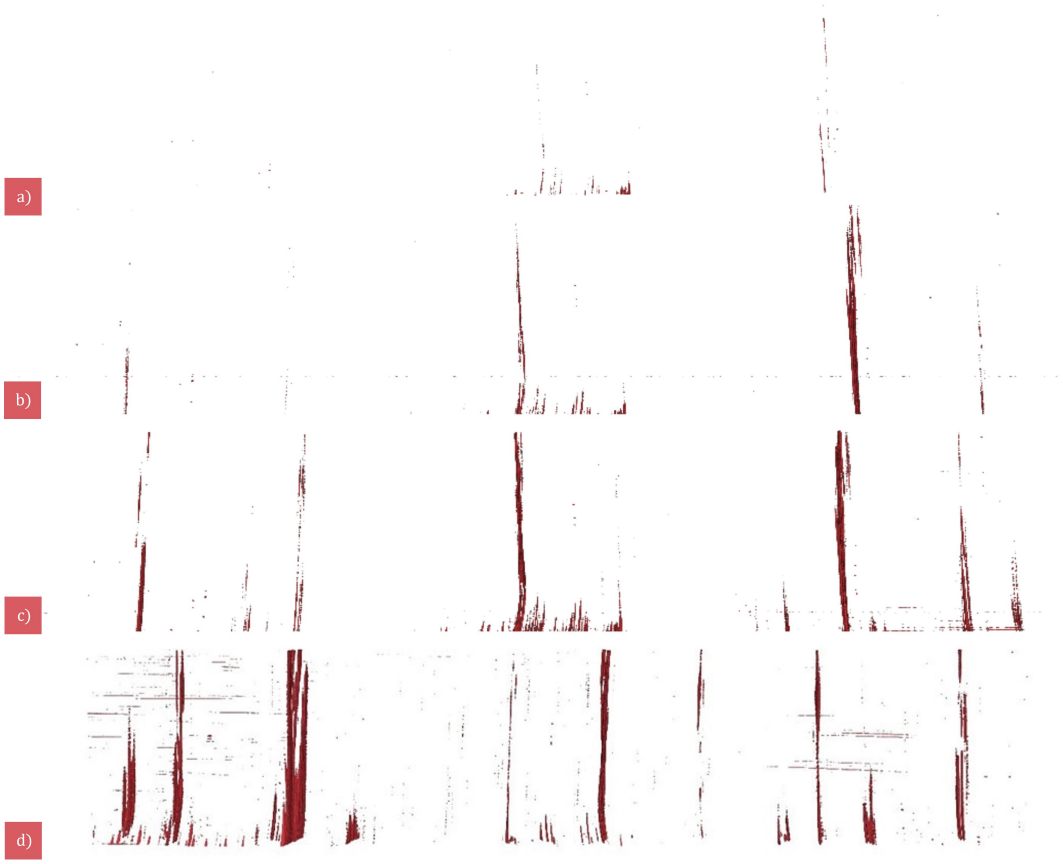


**Figure 5.7:** Representation of the damaged volume in the material Q3: a) 0% strain, b) 0.3% strain, c) 0.4% strain, and d) 0.5% for the view I.

Through the analysis of the volume sequence represented in figures 5.7 and 5.8, one can verify the appearance of randomly distributed cracks that present a more uniform configuration with the increase of the load percentage. It is observed the formation of cracks with different crack opening displacements. The growth of the cracks occurs essentially from the edge of the specimen towards the centre, wherefore it is not possible to consider the damage constant along the width of the specimen during the propagation phase. The crack propagation across the transversal thickness height occurs at a lower rate. Observing the damaged volume for damage near the ultimate fracture, image d), it is observed that only two cracks exhibit the height of the transverse layer. For higher strain values it is possible to observe the formation of tiny oblique cracks.

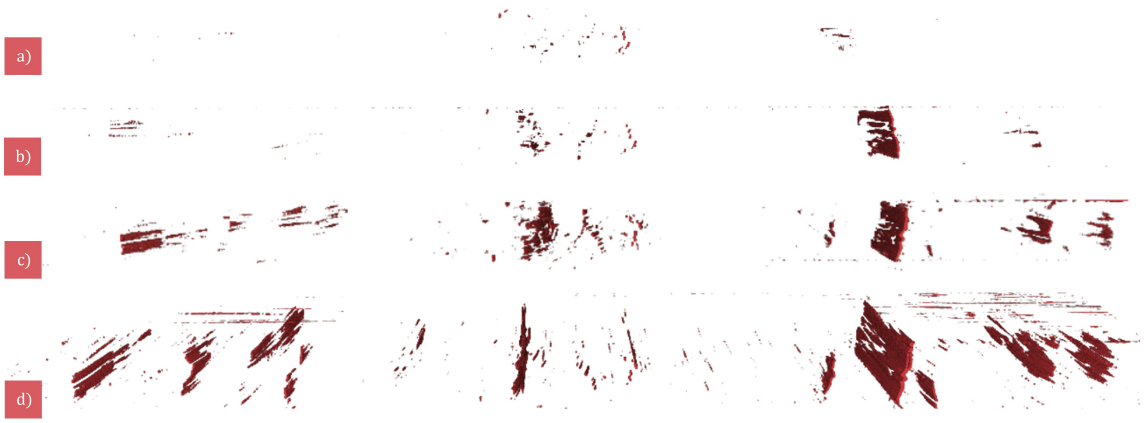


**Figure 5.8:** Representation of the damaged volume in the material Q3: a) 0% strain, b) 0.3% strain, c) 0.4% strain, and d) 0.5% for the view II.

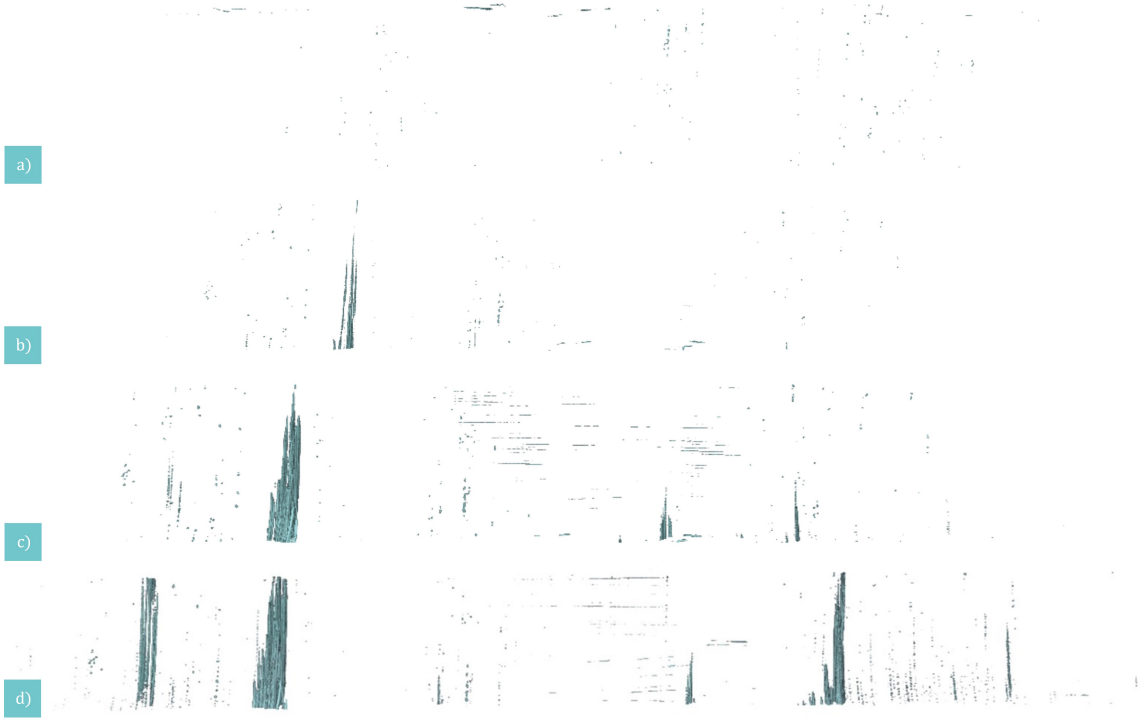


**Figure 5.9:** Representation of the damaged volume in the material Q4: a) 0% strain, b) 0.3% strain, c) 0.4% strain, and d) 0.5% for the view I.

Relatively to the volumes defined for the specimen of intermediate thickness (Figures 5.9 and 5.10), a random distribution in the formation of cracks and a smaller number of cracks are verified. Despite the smaller number of cracks created, it can be verified the existence of a larger damaged volume due to the large dimensions of the cracks. The cracks formed present a vertical orientation and mostly penetrated all the thickness height, contrary to what was observed for the laminate with the thinner transversal layer.

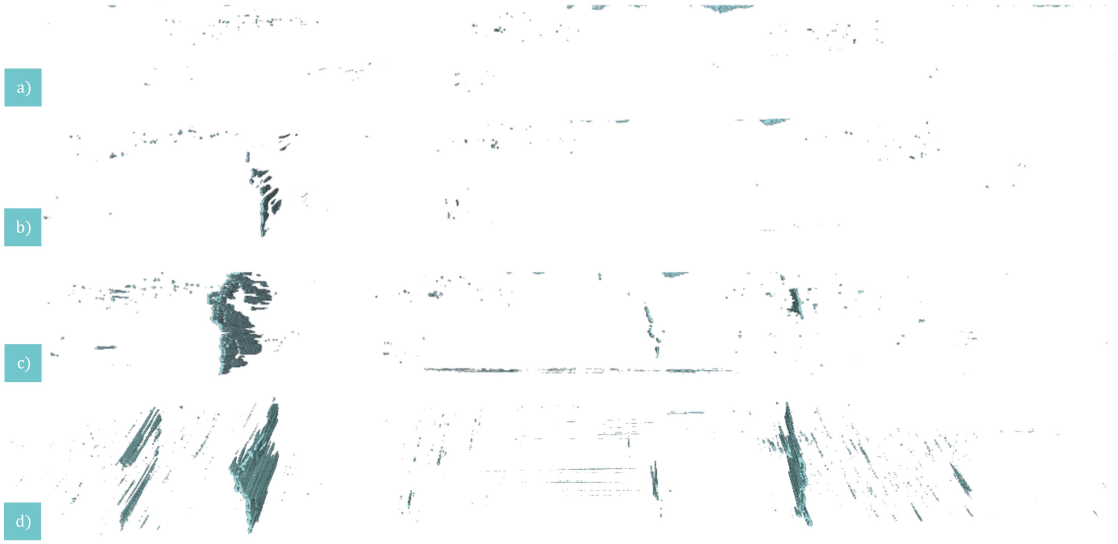


**Figure 5.10:** Representation of the damaged volume in the material Q4: a) 0% strain, b) 0.3% strain, c) 0.4% strain, and d) 0.5% for the view II.

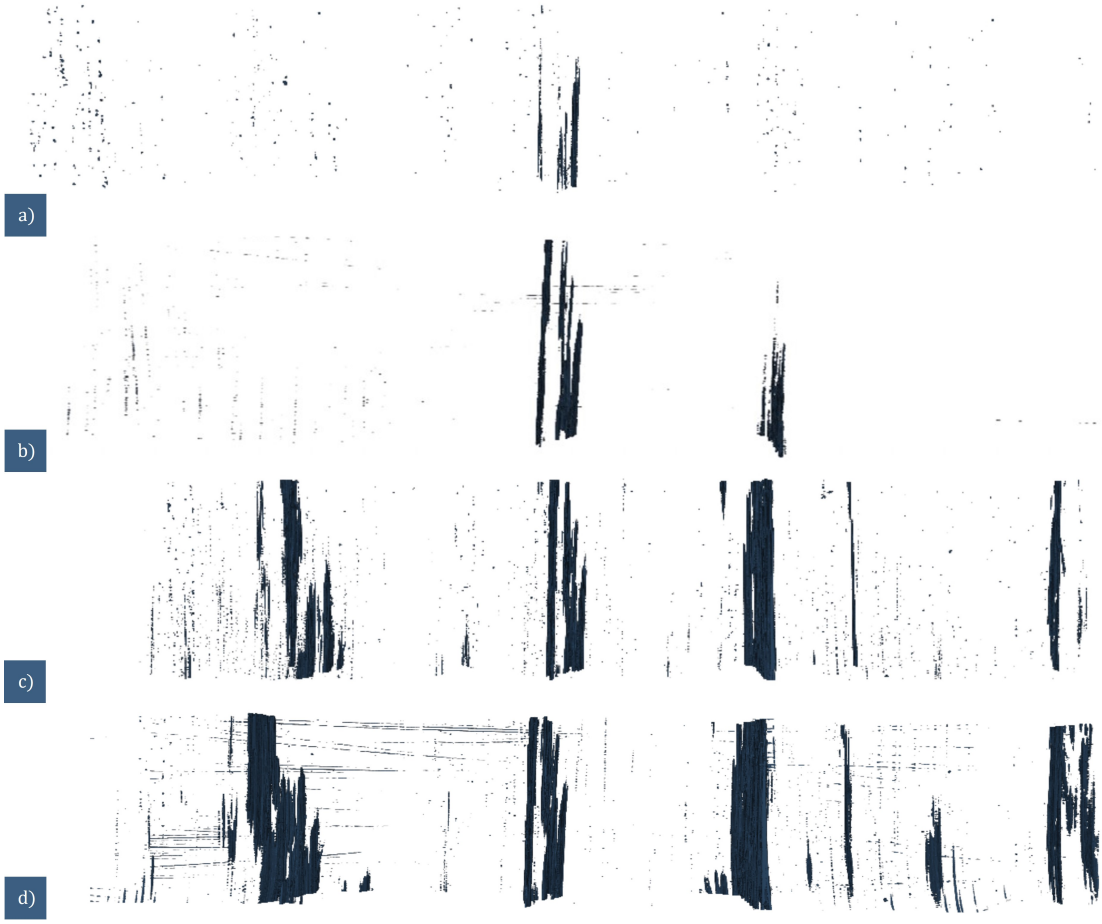


**Figure 5.11:** Representation of the damaged volume in the material Q5: a) 0% strain, b) 0.3% strain, c) 0.4% strain, and d) 0.5% for the view I.

For the thicker laminate (Figures 5.11 and 5.12), it can be seen that the cracks propagate instantly in relation to the specimen width and throughout the entire height of the transversal ply thickness. It is possible to observe a larger damaged volume, distributed throughout the volume under analysis by a low number of cracks with high crack opening displacement.

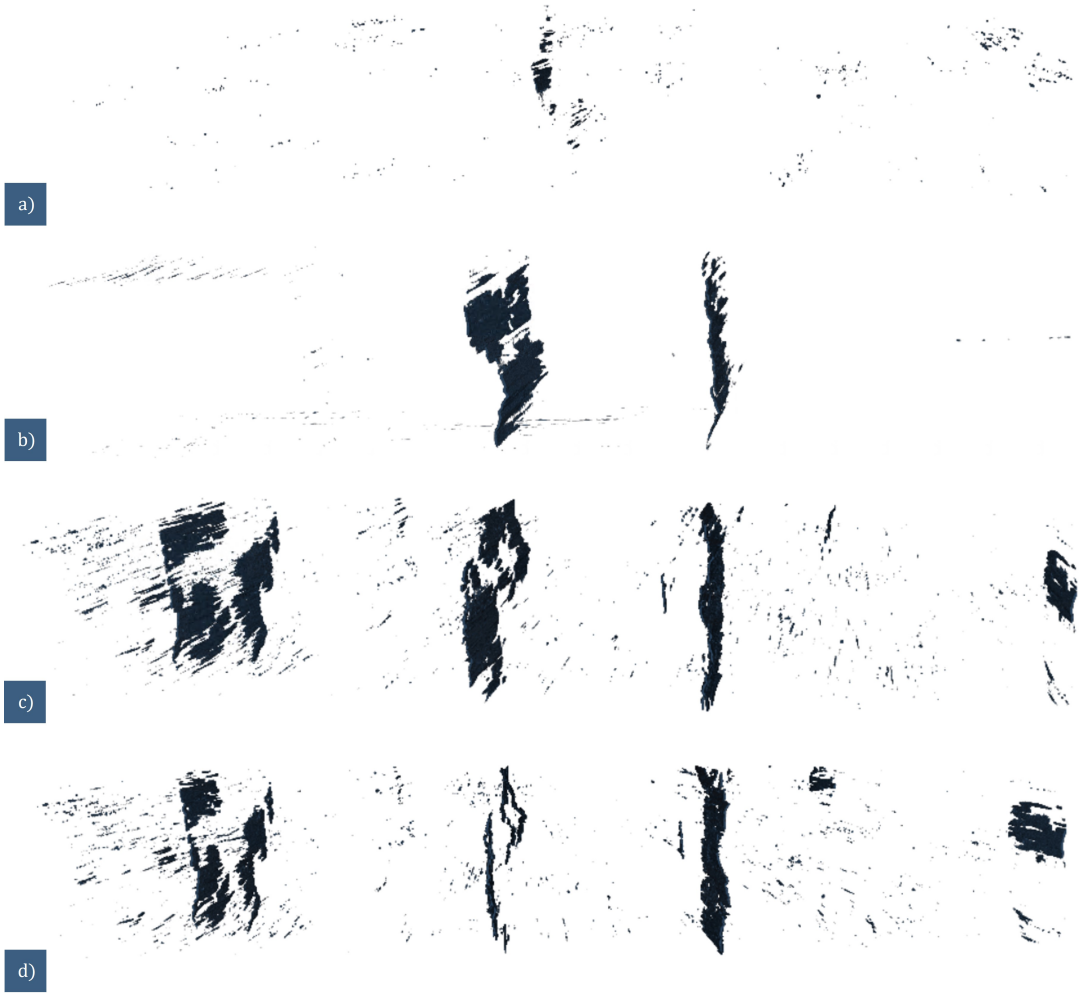


**Figure 5.12:** Representation of the damaged volume in the material Q5: a) 0% strain, b) 0.3% strain, c) 0.4% strain, and d) 0.5% for the view II.

By measuring the damaged volume evolution for each load step it was possible to build the following graph (Figure 5.13). In this way, it is possible to compare the evolution observed for the different configurations, establishing a relation between the damaged volume and the transverse ply thickness for this thermoplastic material.

From the results above it can be concluded that with the increase of the transversal ply thickness, there is a faster propagation of cracks from the edge to the interior of the specimen, as well as a faster crack propagation through the ply thickness, similar to what was observed by Matthieu Nicol [58].

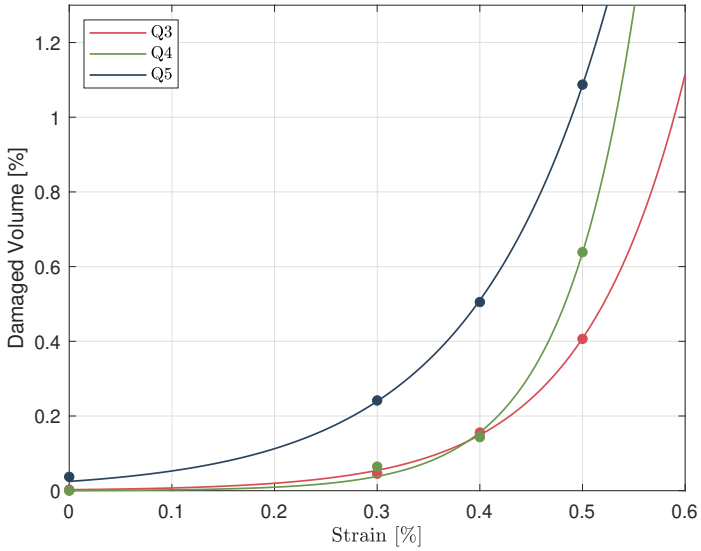


**Figure 5.13:** Damaged Volume as a function of % Strain for different transverse ply thickness.

Observing the plots produced, it can be established a correlation between the onset of damage and the thickness of the transverse plies. As the ply thickness increases it is verified a higher percentage of damaged volume. During the initial loading phase (up to load correspondent to 0.3 of strain) the damage growth rate is relatively slow in comparison to the following loading phases. For the loading step closest to the final failure, the percentage of damaged volume is approximately 1.1 % for the laminate with four transversal plies, 0.65 % for the laminate with two transversal plies and 0.40 % for the laminate with only one transversal ply.

The results obtained for the thermoplastic laminate A in chapter 4 for a two-dimensional edge analysis, do not allow for a representative comparison when comparing the SRCT analysis given the limited and inconsistent data obtained. However, given the similar behaviour of the damage evolution at the edge of the specimens between the studied materials, it is possible to verify a distinct difference regarding the damage evolution observed for volumetric analysis. Having in mind the sudden growth of crack density observed in the previous chapter, the damage growth observed in the volumetric analysis is much slower in an initial phase and later presents an exponential behaviour until fracture.

In comparison with the results of the edge measurements in the previous chapter, this different behaviour affirms the overestimation of the damage state present in the material due to the high damage identified at the edge of the specimens, which for some observed damage corresponds only to a non-passing crack. This behaviour is more pronounced for the thinner laminates, however, with the increase in the thickness of the transverse layer, the existence of non-passing cracks across the whole width is still observed.

# Chapter 6

# Conclusions and Future Work

## 6.1 Conclusion

The main objective of the presented work was to investigate the ply thickness effects on the initiation and propagation of transverse cracking in thermoplastic and thermoset-based composites. To analyze this phenomenon, tension tests were conducted on four different materials, including thermoplastics and two thermosets, for different transverse ply thickness laminates, with *in-situ* capturing of the specimen's edge.

The conducted tests were divided into two methods: continuous tests, which aimed to determine the corresponding tensile strength for each material and interrupted tests, which allowed a clear detection of damage during the loading process.

**Comparation between different laminate configurations of the same material:**

- With the decrease of transverse ply thickness there is an increase of the strength of the onset transversal cracking.
- The evolution of transverse cracking exhibits rapid growth after crack initiation, followed by a decrease in the rate of growth stagnating until the final failure.
- In the finest configurations, it was not possible to see the cracks, as the size of the ply and the resolution of the camera were not adequate.
- Crack spacing decrease until achieving a constant average spacing value. The distribution starts randomly and tends to be a uniform distribution.

**Thermoplastic and thermoset-based composites**

In the results concerning the studied thermoplastics, it was not possible to obtain extensive information that would allow for a valid analysis. However, by comparing the obtained results from the conducted tests, some aspects between the two materials could be distinguished.

By directly comparing thermoset A and B with thermoplastic A, as the cross-ply laminates had the same number of longitudinal plies, a higher stiffness was observed in the thermoplastic matrix specimens. This increased stiffness resulted in a less pronounced effect of ply thickness on the ultimate tensile strength and a slower propagation of damage.

**Effect of manufacture defects**

The effect of manufacturing defects, such as a high content of voids or fibre waviness, was observed and compromised the obtained results for the materials in question. In the analysis of the results for thermoset B, premature delamination was observed, limiting the maximum strength of the material due to the presence of voids near the interfaces between different plies. Regarding the results obtained for the thicker configuration of thermoplastic A, consistency could not be verified due to the presence of in-plane fibre waviness in different sections of the analyzed specimens.

**Synchrotron Radiation Computed Tomography Analysis**

A second study was conducted through the analysis of images obtained from Synchrotron Radiation Computed Tomography tensile tests for thermoplastic material A. In this study, the captured test results were processed and analyzed.

By reconstructing the scanned volumes for different load steps, it was possible to observe the damage related to the propagation of transverse cracks through the thickness and interior of the specimen, leading to the following conclusions:

- The percentage of damage increases with the increase of transverse ply thickness.
- The propagation of damage occurs through a larger number of smaller-sized cracks for thinner laminates, and through larger-sized and higher opening displacement cracks for thicker laminates.
- The propagation of damage from the edge of the specimen to its interior exhibits greater resistance for thinner laminates, with a higher percentage of damage observed near the edge. This resistance is minimized with the increase of the transverse ply thickness of the specimen.

**Crack Density from edge observation length and from analysis volume**

Given the incomplete observation the crack propagation developed at the edge of the specimen through its interior is not observed, the crack density obtained from an analysis based on the edge observation can be considered overestimated, leading to an incorrect assessment of the damage present in the studied material. Therefore, for a more comprehensive analysis, the use of methods such as computed tomography or other more extensive visualization techniques becomes more relevant, as they allow obtaining information about the complete volume under study.

## 6.2 Future Work

Although this thesis provides a robust study on the ply thickness effect on the initiation and propagation of transverse cracking for thermoplastic and thermoset-based composites, there are still issues that should be taken into account for further research. The results obtained for the thermoplastic materials studied did not lead to clear conclusions, so conducting further experimental tests using another imaging detection method would be interesting. In addition to the study conducted for thermoplastic A using Synchrotron Radiation Computed Tomography, performing the same study for a thermoset material would facilitate a comparison between the behaviour of different types of polymer matrix and provide insight into the internal behaviour of both materials.

Interrupted tests at 30 %, 60% and 85 % of failure loads were also carried out on one specimen for each configuration. $\mu$-CT scans were taken at the $\mu$-VIS X-ray Imaging Centre at the University of Southampton to investigate the preliminary damage mechanisms that occur prior to ultimate failure, to achieve a higher resolution visualisation achieving a better understanding of the formation of the crack in the matrix. The results of this analysis are not yet available and, therefore, were not presented in this report.

# References


[1] Hiken A. The evolution of the composite fuselage - a manufacturing perspective. SAE International Journal of Aerospace 2017;10. doi:10.4271/2017-01-2154.

[2] Pérez-Martín H, Mackenzie P, Baidak A, Brádaigh CM, Ray D. Crystallinity studies of pekk and carbon fibre/pekk composites: A review. Composites Part B: Engineering 2021;223.

[3] Pérez-Martín H, Mackenzie P, Baidak A, Brádaigh CM, Ray D. Crystallisation behaviour and morphological studies of pekk and carbon fibre/pekk composites. Composites Part A: Applied Science and Manufacturing 2022;159.

[4] Zweben C. Composite materials. John Wiley  Sons, Inc.; 2015, p. 1–37.

[5] Wang RM, Zheng SR, Zheng YP. In: Wang RM, Zheng SR, Zheng YP, editors. Polymer Matrix Composites and Technology. Woodhead Publishing Series in Composites Science and Engineering; Woodhead Publishing; 2011, p. 1–548.

[6] Liu Y, Zwingmann B, Schlaich M. Carbon fiber reinforced polymer for cable structures—a review. Polymers 2015;7(10):2078–99. URL: https://www.mdpi.com/2073-4360/7/10/1501. doi:10.3390/polym7101501.

[7] Nguyen H, Zatar W, Mutsuyoshi H. 4 - mechanical properties of hybrid polymer composite. In: Thakur VK, Thakur MK, Pappu A, editors. Hybrid Polymer Composite Materials. Woodhead Publishing. ISBN 978-0-08-100787-7; 2017, p. 83–113.

[8] Pethrick R. 9 - composite to metal bonding in aerospace and other applications. In: Chaturvedi M, editor. Welding and Joining of Aerospace Materials (Second Edition); second edition ed. Woodhead Publishing Series in Welding and Other Joining Technologies; Woodhead Publishing. ISBN 978-0-12-819140-8; 2012, p. 277–303.

[9] Mallick PK. Fiber-reinforced composites. Mechanical Engineering; 3 ed.; Boca Raton, FL: CRC Press; 2007.

[10] Ekuase OA, Anjum N, Eze VO, Okoli OI. A review on the out-of-autoclave process for composite manufacturing. Journal of Composites Science 2022;6(6). doi:10.3390/jcs6060172.

[11] Davies L, Day R, Bond D, Nesbitt A, Ellis J, Gardon E. Effect of cure cycle heat

transfer rates on the physical and mechanical properties of an epoxy matrix composite. Composites Science and Technology 2007;67(9):1892–9.

[12] Fernlund G, Rahman N, Courdji R, Bresslauer M, Poursartip A, Willden K, et al. Experimental and numerical study of the effect of cure cycle, tool surface, geometry, and lay-up on the dimensional fidelity of autoclave-processed composite parts. Composites Part A: Applied Science and Manufacturing 2002;33(3):341–51.

[13] Park C, Lee W. 3 - compression molding in polymer matrix composites. In: Advani SG, Hsiao KT, editors. Manufacturing Techniques for Polymer Matrix Composites (PMCs). Woodhead Publishing Series in Composites Science and Engineering; Woodhead Publishing. ISBN 978-0-85709-067-6; 2012, p. 47–94. URL: https://www.sciencedirect.com/science/article/pii/B9780857090676500031. doi:https://doi.org/10.1533/9780857096258.1.47.

[14] Choupin T, Debertrand L, Fayolle B, Regnier G, Paris C, Cinquin J, et al. Influence of thermal history on the mechanical properties of poly(ether ketone ketone) copolymers. POLYMER CRYSTALLIZATION 2019;2. doi:10.1002/pcr2.10086.

[15] McCarthy C, Vaughan T. 14 - micromechanical failure analysis of advanced composite materials. In: Camanho PP, Hallett SR, editors. Numerical Modelling of Failure in Advanced Composite Materials. Woodhead Publishing Series in Composites Science and Engineering; Woodhead Publishing; 2015, p. 379–409.

[16] Jollivet T, Peyrac C, Lefebvre F. Damage of composite materials. Procedia Engineering 2013;66:746–58. Fatigue Design 2013, International Conference Proceedings.

[17] Maimí P, Camanho P, Mayugo J, Dávila C. A continuum damage model for composite laminates: Part i – constitutive model. Mechanics of Materials 2007;39(10):897–908.

[18] Park SY, Choi WJ. Review of material test standardization status for the material qualification of laminated thermosetting composite structures. Journal of Reinforced Plastics and Composites 2021;40(5-6):235–58.

[19] Daniel I, Ishai O. Engineering Mechanics of Composite Materials. No. vol. 13 in Engineering mechanics of composite materials; Oxford University Press; 2006. ISBN 9780195150971. URL: https://books.google.pt/books?id=x5S_QgAACAAJ.

[20] Zhao L, Qin T, Zhang J, Chen Y. 3d gradual material degradation model for progressive damage analyses of unidirectional composite materials. Mathematical Problems in Engineering 2015;2015:1–11. doi:10.1155/2015/145629.

[21] Kreculj D, Rasuo B. Impact damage modeling in laminated composite aircraft structures. ISBN 9780081021316; 2018, p. 125–53. doi:10.1016/B978-0-08-102131-6.00007-4.

[22] Pinho S, Robinson P, Iannucci L. Fracture toughness of the tensile and compressive fibre failure modes in laminated composites. Composites Science and Technology 2006;66(13):2069–79.

[23] Abrate S. Matrix cracking in laminated composites: A review. Composites Engineering 1991;1(6):337–53.

[24] Camanho PP, Dávila CG, Pinho ST, Iannucci L, Robinson P. Prediction of in situ strengths and matrix cracking in composites under transverse tension and in-plane shear. Composites Part A: Applied Science and Manufacturing 2006;37(2):165–76. CompTest 2004.

[25] Dvorak GJ, Laws N. Analysis of progressive matrix cracking in composite laminates ii. first ply failure. Journal of Composite Materials 1987;21(4):309–29.

[26] Laws N, Dvorak GJ. Progressive transverse cracking in composite laminates. Journal of Composite Materials 1988;22(10):900–16.

[27] Berthelot JM, Le Corre JF. Statistical analysis of the progression of transverse cracking and delamination in cross-ply laminates. Composites Science and Technology 2000;60(14):2659–69.

[28] Highsmith A, Reifsnider K, International A, for Testing AS, Materials . Stiffness-Reduction Mechanisms in Composite Laminates. ASTM International; 1982.

[29] Carraro PA, Novello E, Quaresimin M, Zappalorto M. Delamination onset in symmetric cross-ply laminates under static loads: Theory, numerics and experiments. Composite Structures 2017;176:420–32.

[30] Parvizi A, Bailey JE. On multiple transverse cracking in glass fibre epoxy cross-ply laminates. Journal of Materials Science 1978;13:2131–6.

[31] Flaggs DL, Kural MH. Experimental determination of the in situ transverse lamina strength in graphite/epoxy laminates. Journal of Composite Materials 1982;16(2):103–16.

[32] Ye J, Lam D, Zhang D. Initiation and propagation of transverse cracking in composite laminates. Computational Materials Science 2010;47(4):1031–9.

[33] Pinho S, Dávila C, Camanho P, Iannucci L, Robinson P. Failure models and criteria for frp under in-plane or three-dimensional stress states including shear non-linearity 2005;.

[34] Dávila C, Rose C, Iarve E. Modeling fracture and complex crack networks in laminated composites 2013;5.

[35] Arteiro A, Catalanotti G, Melro A, Linde P, Camanho P. Micro-mechanical analysis of the in situ effect in polymer composite laminates. Composite Structures 2014;116:827–40.

[36] Saito H, Takeuchi H, Kimpara I. Experimental evaluation of the damage growth restraining in 90° layer of thin-ply cfrp cross-ply laminates. Advanced Composite Materials - ADV COMPOS MATER 2012;21:57–66.

## References


[37] Garrett KW, Bailey JE. Multiple transverse fracture in 90 o cross-ply laminates of a glass fibre-reinforced polyester. JOURNAL OF MATERIALS SCIENCE 1977;12:157–68.

[38] Parvizi A, Rett KWG, Bailey JE. Constrained cracking in glass fibre-reinforced epoxy cross-ply laminates. 1978.

[39] Liu S, Nairn JA. The formation and propagation of matrix microcracks in cross-ply laminates during static loading. Journal of Reinforced Plastics and Composites 1992;11(2):158–78.

[40] Boniface L, Smith P, Bader M, Rezaifard A. Transverse ply cracking in cross-ply cfrp laminates - initiation or propagation controlled? JOURNAL OF COMPOSITE MATERIALS 1997;31(11):1080 –112.

[41] Silberschmidt VV. Matrix cracking in cross-ply laminates: effect of randomness. Composites Part A: Applied Science and Manufacturing 2005;36(2):129–35. doi:https://doi.org/10.1016/j.compositesa.2004.06.008; 7th International Conference on the Deformation and Fracture of Composites (DFC-7).

[42] Aveston J, Kelly A. Theory of multiple fracture of fibrous composites. Journal of Materials Science 1973;8(3):352–62.

[43] Flaggs D. Prediction of tensile matrix failure in composite laminates. Journal of Composite Materials 1985;19(1):29–50.

[44] ???? URL: https://www.thinplytechnology.com/assets/mesimages/NTPT-DS-ThinPreg-736LT-v2.pdf.

[45] ???? URL: https://shdcomposites.com/admin/resources/datasheets/frvc411-tds-2.pdf.

[46] Sisodia S, Gamstedt K, Edgren F, Varna J. Effects of voids on quasi-static and tension fatigue behaviour of carbon-fibre composite laminates. Journal of Composite Materials 2014;49. doi:10.1177/0021998314541993.

[47] Mehdikhani M, Steensels E, Standaert A, Vallons KA, Gorbatikh L, Lomov SV. Multi-scale digital image correlation for detection and quantification of matrix cracks in carbon fiber composite laminates in the absence and presence of voids controlled by the cure cycle. Composites Part B: Engineering 2018;154:138–47. URL: https://www.sciencedirect.com/science/article/pii/S1359836818309260. doi:https://doi.org/10.1016/j.compositesb.2018.07.006.

[48] Mehdikhani M, Petrov NA, Straumit I, Melro AR, Lomov SV, Gorbatikh L. The effect of voids on matrix cracking in composite laminates as revealed by combined computations at the micro- and meso-scales. Composites Part A: Applied Science and Manufacturing 2019;117:180–92. doi:https://doi.org/10.1016/j.compositesa.2018.11.009.

[49] Talreja R. Studies on the failure analysis of composite materials with manufacturing defects. Mech Compos Mater 2013;49(1):35–44.

[50] Huang Y, Varna J, Talreja R. Statistical methodology for assessing manufacturing quality related to transverse cracking in cross ply laminates. Composites Science and Technology 2014;95:100–6. doi:https://doi.org/10.1016/j.compscitech.2014.02.010.

[51] Makeev A, Seon G, Lee E. Failure predictions for carbon/epoxy tape laminates with wavy plies. Journal of composite materials 2010;44(1):95–112.

[52] Zhao C, Xiao J, Li Y, Chu Q, Xu T, Wang B. An experimental study of the influence of in-plane fiber waviness on unidirectional laminates tensile properties. Appl Compos Mater 2017;24(6):1321–37.

[53] Bloom L, Wang J, Potter K. Damage progression and defect sensitivity: An experimental study of representative wrinkles in tension. Composites Part B: Engineering 2013;45(1):449–58. doi:https://doi.org/10.1016/j.compositesb.2012.05.021.

[54] Krämer E, Grouve W, Koussios S, Warnet L, Akkerman R. Real-time observation of waviness formation during c/peek consolidation. Composites Part A: Applied Science and Manufacturing 2020;133:105872. URL: https://www.sciencedirect.com/science/article/pii/S1359835X2030110X. doi:https://doi.org/10.1016/j.compositesa.2020.105872.

[55] Kulkarni P, Mali KD, Singh S. An overview of the formation of fibre waviness and its effect on the mechanical performance of fibre reinforced polymer composites. Composites Part A: Applied Science and Manufacturing 2020;137:106013. doi:https://doi.org/10.1016/j.compositesa.2020.106013.

[56] Swolfs Y, Morton H, Scott A, Gorbatikh L, Reed P, Sinclair I, et al. Synchrotron radiation computed tomography for experimental validation of a tensile strength model for unidirectional fibre-reinforced composites. Composites Part A: Applied Science and Manufacturing 2015;77:106–13. doi:10.1016/j.compositesa.2015.06.018.

[57] Borstnar G, Mavrogordato M, Helfen L, Sinclair I, Spearing S. Interlaminar fracture micro-mechanisms in toughened carbon fibre reinforced plastics investigated via synchrotron radiation computed tomography and laminography. Composites Part A: Applied Science and Manufacturing 2015;71:176–83. doi:https://doi.org/10.1016/j.compositesa.2015.01.012.

[58] Nicol M. Compréhension et modélisation de l'influence de l'ordre d'empilement sur les scénarios d'endommagement dans des composites stratifiés de plis unidirectionnels. Ph.D. thesis; e l'université Paris-Saclay; 2023.